Official Journal of WORLD FOUNDRYMEN ORGANIZATION (WFO)

GIESSEREIFORSCHUNG
International Foundry Research

1/2008

Reprint from „Foundry Research/Giessereiforschung“ Volume 60 (2008), issue No. 1 page 2-19

Giesserei-Verlag GmbH · Postfach 10 25 32 · 40016 Düsseldorf
PVSt, Deutsche Post AG, Entgelt bezahlt, G 57454 Heft 1/2008

GIESSEREIFORSCHUNG 60 (2008) No. 1
Pp. 2–66; 1 Quarter; ISSN 0046-5933

The use of oxygen activity measurement to determine optimal properties of ductile iron during production

Oxygen activity in ductile cast iron melts with ferritic and pearlitic structure has been measured as a function of the time while keeping the furnace temperature approximately constant around 1420 °C.
A commercially available sensor, improved very recently, has been employed. The measurements are done in a 250 kg capacity induction furnace representing industrial circumstances.
In ductile iron, oxygen activity measurements permit a determination of an optimal melt condition. Castings poured in these circumstances present maximal nodularity, elongation and ferrite content combined with lowest hardness.

Frans Mampaey, Zwijnaarde, Belgium,
Danny Habets, Jaques Plessers and
Frank Seutens, Houthalen, Belgium

Manuscript received 25 October 2007;
accepted 8 November 2007

F. Mampaey, Sirris Materials Processing, Zwijnaarde, Belgium, **D. Habets**, **J. Plessers** and **F. Seutens**, Heraeus Electro-Nite, Houthalen, Belgium

1 Introduction

Oxygen can be present in a cast iron melt in two different forms: as a solute element or bound as an oxide, varying from simple to complex compounds. The oxygen in solution influences liquid properties, for example, the surface tension. More importantly, it also affects the morphology of graphite during solidification. Soluble oxygen content cannot be measured directly in liquid cast iron. However, special sensors provide us with an opportunity to determine the oxygen activity. As will be shown later, the calculation of the amount of oxygen in solution from the oxygen activity is theoretically well established. In practice, the conversion may be questionable because accurate correction factors, needed for multicomponent alloys are lacking. Oxides, which are the second form of oxygen in the melt, are directly related to the heterogeneous nucleation sites and to slag formation. The scanning electron microscope has permitted identification of inclusions within graphite particles. Many of these nucleation sites have a complex structure and contain oxides. The amount and type of oxides can be measured using hot extraction techniques. Unfortunately, these techniques are laborious and not common in foundry practice.

The total amount of oxygen in a cast iron base melt depends on the melting method. Usually, total oxygen content is somewhat lower in induction melted cast iron (30 to 80 ppm) than in cupola melted cast iron (70 to 150 ppm). In gray iron, the oxide content may vary considerably from charge to charge. The total combined oxygen is present in different form which can be derived from the hot extraction technique. For a total oxygen content of 105 ppm, E. Hofmann and G. Wolf [1] found about 50 percent oxygen present as SiO_2, 8 ppm as FeO + MnO, the rest being bound as silicates, mixed oxides or oxides decomposing at higher temperature than SiO_2, (for example Al_2O_3 or TiO_2) . The authors note that superheating and subsequent holding of a melt reduces the total oxygen content from 106 ppm after melting down to 48 ppm. In hypereutectic gray iron, Y. Lerner [2] did not find noticeable changes of the oxygen content in the course of the production process: 55 ppm (cupola iron), 51 ppm (holding furnace iron) and 50 to 52 ppm in the castings (permanent mold).

On the other hand, the oxygen activity is much lower and very dependent on the temperature of the melt. For example, just to illustrate the order, in gray iron the oxygen activity in one of the experiments carried out drops from 1.8 ppm at 1480 °C to 0.44 ppm at 1350 °C. The change does not result from a transfer of oxygen atoms from the melt to the air. It originates from the fact that the equilibrium of the chemical reaction

$$Si + 2O \rightarrow SiO_2 \qquad (1)$$

changes with temperature. At higher temperature, the reaction shifts to the left — silicon and oxygen combine less — resulting in more "free" active oxygen in the cast iron melt.

The present paper does not intend to review extensively all publications related to oxygen activity measurements. M. Hecht and R. Hummer have used oxygen activity sensors produced by Heraeus Electro-Nite. M. Hecht and J. B. Loury [3] have examined in great detail the relation between DF (or "deoxidation factor" which is a supplemental value obtained with each measurement) and residual magnesium content. Based on their experimental results, the authors

could not conclude which parameter — emf, oxygen activity or *DF* — is most appropriate to quantitatively characterize a Mg-treated melt. R. Hummer [4] concludes that combined emf (oxygen activity) measurements and thermal analysis are best to discern between lamellar, compacted and spheroidal graphite cast iron. He believes that the oxygen activity value at which transitions between graphite types occur are not absolute values but depend on the measurement and treatment conditions. R. Hummer [5] found that the feeding behavior of ductile iron improves and external sinking decreases when the oxygen activity increases. M. Morinaka e. a. [6] examined several parameters, including oxygen in solution, during solidification of melts with variable magnesium content. They did not directly relate oxygen activity with the different graphite types (spheroidal, vermicular and lamellar). The authors published a relationship between the growth rates of all graphite eutectics and the undercooling. Other references will be mentioned later in the paper.

2 Oxygen activity sensor

2.1 Measurement principle

A commercial sensor (ref. [7] "foundry sensor") determines the oxygen activity using an electrochemical cell and a Pt-PtRh thermocouple. The sensor comprises Cr-Cr_2O_3 as the reference cell and zircon stabilized with Mg as a solid-state electrolyte. Once the sensor is immersed in the bath an electrochemical cell is formed; one compartment being the reference cell, the other compartment the melt. This device converts chemical energy to electrical energy because the oxygen potential is different in both compartments. Schematically, the complete cell during oxygen activity measurement becomes

negative Mo electrode | Cr + Cr_2O_3 || ZrO_2 (MgO-stabilized) electrolyte ||melt | positive Fe electrode

The cell potential (ε_{cell}) or electromotive force (emf) is given by the Nernst equation

$$\varepsilon_{cell} = \varepsilon^0_{cell} - \frac{RT}{n\mathrm{F}} \ln(Q) \tag{2}$$

where ε^0_{cell} is the standard state cell potential, R is the gas constant, F the Faraday constant, T the Kelvin temperature, n the number of moles of electrons involved in the reaction and Q the reaction quotient.

At equilibrium, Q becomes the equilibrium constant K and ε_{cell} is 0. For the present application, the reaction quotient Q is equal to the ratio between the partial pressure of oxygen in the reference cell and the partial pressure of oxygen in the melt. As for any substance, the activity of oxygen is defined as the ratio of the partial pressure of oxygen to a reference pressure. Hence, Equation (2) provides a relationship between the measured cell potential and the activity of oxygen in the melt. For the present sensor, the manufacturer uses

$$\log a_0 = 8.62 - \{13\,580 - 10.08\,(E + 24)\} / T \tag{3}$$

with E in mV and a_0 in ppm.

Sensors, which measure activities based on the Nernst equation, have the advantage to be very sensitive at low concentrations, as the potential is related logarithmically to the concentration [8].

2.2 Representation of results

The thermodynamics involved in oxygen activity measurements have been discussed in detail in a previous publication [9] and will only be briefly recalled here with the intention to explain how and why experimental results are represented graphically. We will illustrate this for the oxidation of Si in liquid iron

$$\frac{1}{2}[\mathrm{Si}] + [\mathrm{O}] \rightarrow \frac{1}{2}\langle \mathrm{SiO_2} \rangle \tag{4}$$

where Si and O are in solution (activities of Henry, symbol []) and SiO_2 is present as a solid (activity of Raoult, symbol <>).

The Standard Gibbs energy ΔG^0 for a chemical reaction is

$$\Delta G^0 = \Delta H^0 - T\Delta S^0 \tag{5}$$

where H is the enthalpy, S the entropy and T the absolute (Kelvin) temperature. Equation (5) pertains to Si and O in solution in liquid iron. It may be derived from the reaction between the pure components silicon and oxygen by including ΔG^0 for the melting of silicon and by taking into account the change in Standard Gibbs energy when 1 mole of the pure substance is dissolved to 1 mass percent in liquid iron.

The change of Gibbs energy for the reaction shown in Equation (4) is

$$\Delta G = \Delta G^0 + \mathrm{R}T \ln\left(\frac{a_{SiO_2}^{1/2}}{a_{Si}^{1/2} a_O}\right) = \Delta G^0 + \mathrm{R}T \ln(Q) \tag{6}$$

where R is the gas constant and Q the reaction quotient. At chemical equilibrium, ΔG is equal to 0 and Q becomes the equilibrium constant K. Combining Equations (5) and (6) for equilibrium, and changing from the natural logarithm (ln) to the logarithm base 10 (log) gives

$$\log a_O = -15434\frac{1}{T} + 5.98 - \frac{1}{2}\log a_{Si} + \frac{1}{2}\log a_{SiO_2} \tag{7}$$

In general, the concentration of an element i [i %*] is not equal to the corresponding activity a_i but related by the activity coefficient (of Henry, in case of mass percent concentration). Moreover, the activity of solute B in the solvent A will be influenced by the presence of other solutes C, D,…, N. The Henrian activity coefficient of B in the complex solution (B, C, D,…, N in A) will be different from the one valid for the binary solution (B in A). This effect may be taken into account by the introduction of interaction coefficients. Details of this procedure have been published before [9]. However, the introduction of interaction coefficients does not influence the temperature dependent part in the previous equation, but only changes the temperature independent

*Unless specified otherwise, the composition percentages indicate mass fractions.

part. Consequently, the relation between oxygen activity and temperature is given as

$$\log a_O = \text{coefficient}\,\frac{1}{T} + \text{C} \tag{8}$$

where the constant C in the equilibrium equation changes with the content of the element involved (Al, Si, Mg), with the possible interaction between the elements present and with the activity of the corresponding oxide. As will be shown later in the paper, oxygen activity largely changes with temperature. Consequently, measured oxygen activities will be recalculated to a constant reference temperature of 1420 °C using Equation (8). Detailed conversion data will be given later (Table 2).

2.3 Expected behavior

The present research aims to examine oxygen activity for the case of ductile iron. The relation for oxygen activity in the presence of magnesium is given by:

$$\log a_O = -25751\frac{1}{T} + 6.28 - \log a_{Mg} + \log a_{MgO} \tag{9}$$

Data to derive this equation are taken from T. A. Engh [10]. R. Hummer [5] has published an equation based on unpublished research of R. Schlüsselberger which is valid for iron melts

$$\log\left\{[\text{O}][\text{Mg}]\right\} = -24973\frac{1}{T} + 7.36 \tag{10}$$

where [O] and [Mg] represent oxygen and magnesium in solution (mass percent).

Plotting oxygen activity as a function of magnesium permits a visualization of the expected behavior when the magnesium content of the bath varies at a constant temperature. Application of Equations (9) or (10) results in oxygen activity data which are much lower than measured (**Figure 1**). For example, Equation (10) gives 0.008 ppm oxygen for 0.05 percent magnesium at 1420 °C. The reason for the discrepancy derives from the fact that the theoretical equations are valid for equilibrium between pure components, present in sufficient quantity. This is represented by the equation for chemical equilibrium

$$\ln\frac{a_O\, a_{Mg}}{a_{MgO}} = \ln \text{K} = -\frac{\Delta G^0}{\text{R}T} \tag{11}$$

where ΔG^0 is the Standard Gibbs energy for this reaction and K the equilibrium constant.

The experimental data from Figure 1 indicate that about 0.7 ppm oxygen is available in the melt prior to magnesium addition. When a certain quantity of magnesium is added to the melt, equilibrium is established taking into account the available amount of each component. Rather than solving the theoretical Equation (11) for chemical equilibrium, we need to solve the equation below which takes into account limited initial quantities of magnesium and oxygen

$$\ln\frac{\langle \text{O} - x\rangle\langle \text{Mg} - x\rangle}{x} = \ln \text{K} = -\frac{\Delta G^0}{\text{R}T} \tag{12}$$

where x is the mole fraction of oxygen reacting with magnesium. Equation (12) has been solved with the numerical data of Equation (9) for an initial oxygen activity of 0.7 ppm and a constant activity of MgO equal to 0.3. This result is shown by the solid curve in Figure 1. For very low magnesium contents (<0.0065 %), the assumption of a constant activity for MgO does not hold because MgO decomposes — and as such decreases its activity — to establish equilibrium. It is represented by the dashed curve of Figure 1. Finally, it should be noted that the experimental data in Figure 1 are residual magnesium contents. The true active magnesium content is lower than the residual magnesium content because the latter also includes MgO and MgS.

Consequently, Figure 1 should only be used for illustrative purposes. Most importantly, theory shows that oxygen activity asymptotically decreases at high magnesium levels.

3 Summary of previous research

Recently, one of the authors has published results which were based on research carried out with the first version of the Foundry Sensor [9]. The results from this research will be summarized here.

3.1 Difference with equilibrium measurements

In the present experiments as well as during industrial practice, the effect of magnesium after its addition to the melt occurs relatively quickly. About one or two minutes after magnesium addition, a large quantity of liquid is homogenized and equilibrium in the melt is established. The equilibrium of the magnesium-oxygen reaction is probably reached sooner because time is needed to mix magnesium into a homogeneous solution. A. Mihajlovic [11] and J. Wang [12] also noted that oxygen content cannot be increased because it reacts immediately. In combination with a proper inoculation, it permits to produce castings with a homogeneous spheroidal graphite structure soon after treatment. Moreover, magnesium treatment is carried out in relatively large furnaces which makes that most of the liquid will not come in contact with the furnace wall in the short time after the magnesium treatment. However, as shown by the chemical reaction

$$[\text{Mg}] + [\text{O}] \rightarrow \langle \text{MgO}\rangle \tag{13}$$

equilibrium requires the presence of a solid oxide. Obviously, this cannot be the furnace wall.

The present and commonly used industrial practice is quite in contrast with true equilibrium activity measurements (for example [13]). In these conditions, a small quantity of melt (four grams) is made from very pure base materials. The liquid is kept in contact with the pure reaction product using clean crucibles. Several hours are waited under controlled atmosphere in order to reach equilibrium before measurement starts.

3.2 Nature of the solid oxide reaction product

How can we reach equilibrium within two minutes after the magnesium addition?

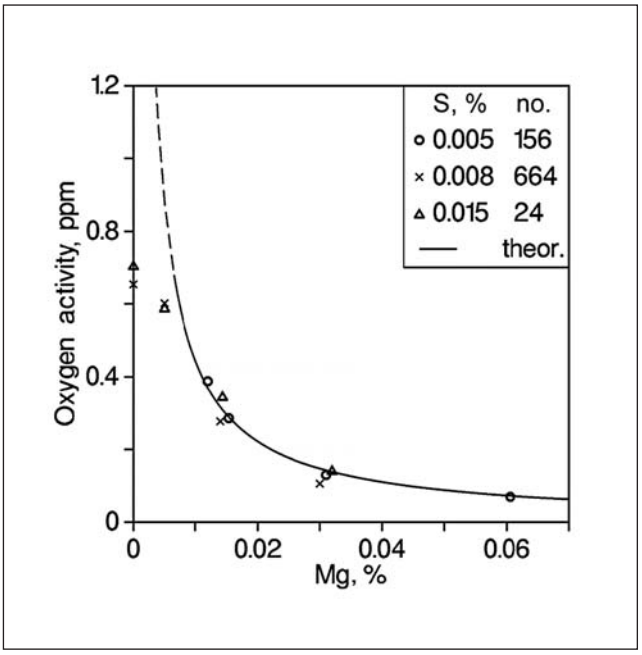

Figure 1: Oxygen activity at 1420 °C as a function of residual Mg content for heats with different S content. The curve shows the theoretical relation as given by Equation (9) for a total oxygen content of 0.7 ppm (results obtained with the old version of the Foundry Sensor).

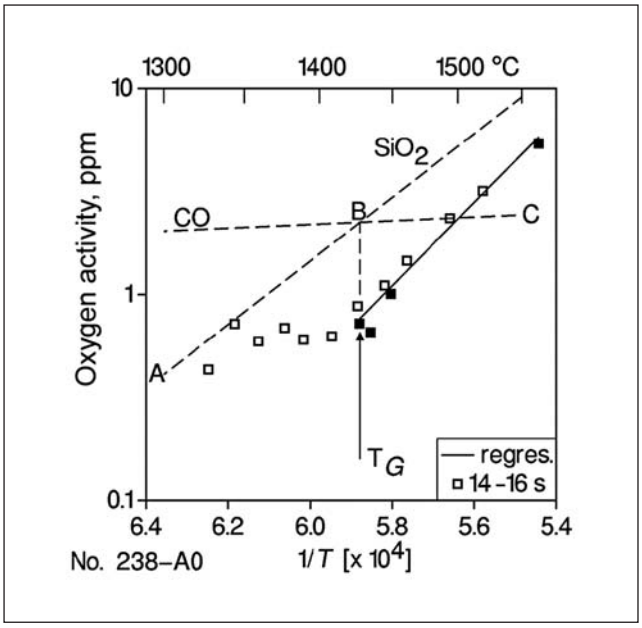

Figure 2: Oxygen activity as a function of temperature in the absence of Mg and 0.1 % Ti [9]. Measurements during heating up the melt are shown as solid symbols. Lines CO and SiO_2 show the oxygen activity according to Equations (16) and (7); T_G is the equilibrium temperature for reduction of silicon dioxide by carbon (Equation (17)) (results obtained with the old version of the Foundry Sensor)

Obviously, the solid oxide in Equation (13) is provided by the heterogeneous nucleation substrates present in the melt. The heterogeneous substrates are small and occur in very high volumetric counts. In an inoculated ductile iron casting, the number of nodules measured is $6.7 \times 10^{13}/m^3$ which is about 14 percent of the available nucleation sites ($5.0 \times 10^{14}/m^3$) [14]. It explains why chemical equilibrium can be reached in a microscopic volume within the melt without the need for the melt to be in contact with the furnace or vessel wall. The consequence of this hypothesis is, however, that the solid oxide will not be a pure substance. Indeed numerous research devoted to determining the crystallographic nature of the heterogeneous nucleation sites has pointed to rather complex mixtures. This is true for gray iron as well as magnesium (or Rare Earth) treated ductile iron.

In lamellar graphite cast iron, oxygen is in equilibrium with silicon (Equation (4)). Solid SiO_2 is probably present in the melt as a mixture in compound oxides or even in more complex combinations with sulfides and/or silicates.

In the case of gray iron, when magnesium is absent, M. Chisamera e. a. [15] noted that SiO_2 is not an effective substrate for graphite nucleation. However, other elements such as Ca, Al and Ti can transform SiO_2 into favorable nucleation sites. T. Skaland e. a. [16] have examined the nature of inclusions after nodulization but before inoculation, which corresponds to the present experimental conditions. $MgO \cdot SiO_2$ or $2MgO \cdot SiO_2$ can form and coexist over a relatively wide composition range. Moreover, $MgO \cdot SiO_2$ may contain considerable amounts of Al_2O_3 in solid solution supporting the hypothesis that the activity of solid oxide may be lower than unity because it is present as a mixture and not as a pure oxide. This is illustrated in **Figure 2** for gray iron. The solid line in the Figure is given by Equation (7) if the activity of solid silicon dioxide is equal to 0.12 at 1428 °C.

3.3 Reduction of SiO_2 by carbon is too slow to be measured

Figure 2 also shows the theoretical equilibrium oxygen activity given by two chemical reactions. The first is the reaction of silicon and oxygen in liquid iron (Equation (7)). In this equation silicon activity is calculated using the interaction coefficients (Equation (14)) while the activity of silicon dioxide is taken as one, assuming a pure compound.

$$a_{Si} = f_{Si}^{Si} \times f_{Si}^{C} \times f_{Si}^{O} \times [\%Si] = \\ = 1.66 \times 4.09 \times 0.9997 \times 2 = 13.58 \quad (14)$$

The second equation concerns the equilibrium between carbon and oxygen in liquid iron:

$$[C] + [O] \leftrightarrow \{CO\} \quad (15)$$

The product CO is gaseous with a partial pressure set to 1 atm. for the calculation of the oxygen activity and a_C = 0.4 × C %:

$$\log\left(\frac{a_O \, a_C}{p_{CO}}\right) = \frac{-896}{T} - 2.21 \quad (16)$$

Figure 2 also shows the equilibrium temperature for the reduction of SiO_2 by carbon (T_G), as given by Orths e. a. [17]:

$$\log\left(\frac{Si\%}{(C\%)^2}\right) = \frac{-27486}{T} + 15.47 \quad (17)$$

with silicon and carbon in mass percent and T the Kelvin temperature. For the composition of Figure 2 (3.28 % C, 2.2

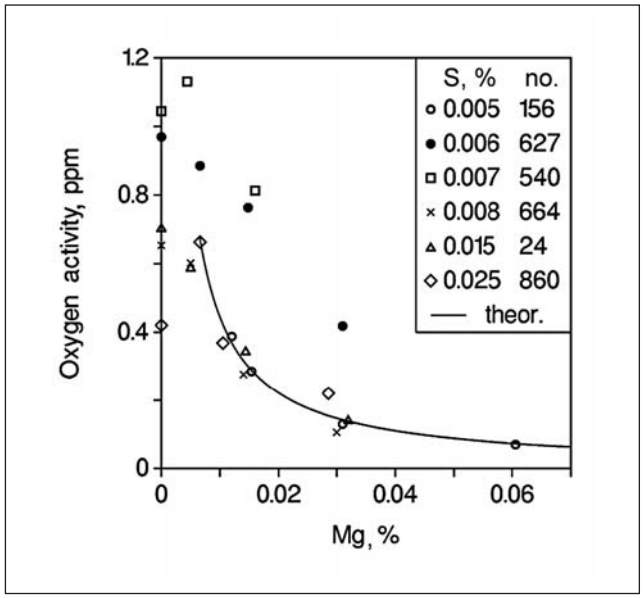

Figure 3: Oxygen activity as a function residual Mg content for heats with different S content [9]. The solid curve shows the theoretical relation as given by Equation (9) (results obtained with the old version of the Foundry Sensor).

% Si) Equation (17) gives 1428 °C which is on the intersection of Equations (7) and (16). The temperature for the reduction of SiO_2 by carbon can be measured from experimental observation [18] while Equations (7) and (16) comprise several parameters (interaction coefficients, activity of SiO_2 and CO) for which the exact value may be uncertain for cast iron.

According to thermodynamics, the reaction product with lowest free energy will be most stable. In the present case this is silicon dioxide below T_G and CO above this temperature. Consequently, oxygen activity should follow the lines between points A, B and C in Figure 2. Below the equilibrium temperature for the reduction of SiO_2 by carbon (T_G), oxygen activity varies between A and B. At higher temperature, no silicon dioxide is formed and Equation (16) should determine the oxygen activity (line BC). The slope of the line BC is rather low. About 60 °C above the equilibrium temperature for the reduction of SiO_2 by carbon, CO gas bubbles

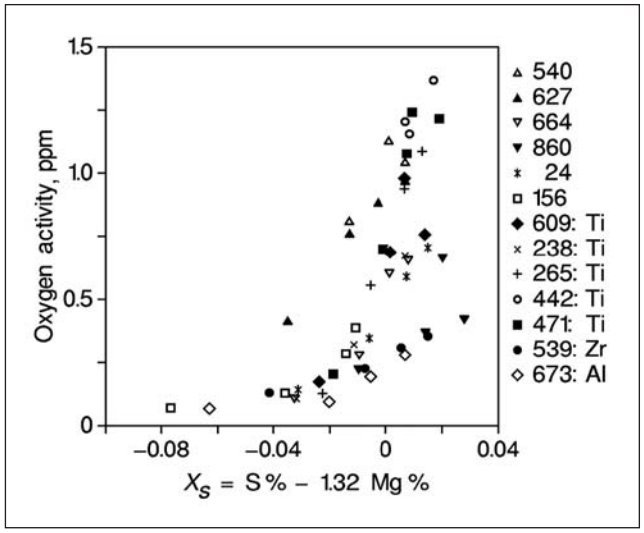

Figure 4: Oxygen activity at 1420 °C as a function of X_s [9] (results obtained with the old version of the Foundry Sensor)

form and carbon content of the melt decreases (temperature T_K). K. Orths e. a. [19] have published an equation for T_K.

$$T_K = 0.7866\ T_G + 362 \qquad \text{[degrees C]} \qquad (18)$$

The measured oxygen activity differs substantially from the expected theoretical behavior. Above the equilibrium temperature for the reduction of SiO_2 by carbon (T_G) oxygen activity depends on the oxidation of silicon (Equation (7)) even when the temperature is higher than T_K. In all experiments carried out with only silicon present in the melt as reactant with oxygen (i. e. in the absence of Mg, Ti, Al or Zr) an arrest in oxygen activity, parallel to the line BC due to CO formation, was never noticed. Other researchers have noticed the same behavior [20].

There is another argument — reaction rate — which provides an explanation as to why carbon does not control oxygen activity above T_G, the equilibrium temperature. Equations (7) and (16) define the chemical equilibrium but tell nothing about the rate at which equilibrium is established. Experiments of T. Kusakawa [21] and E. Hofmann and G. Wolf [1] showed that holding a melt for about 10 minutes above the temperature T_K does not influence solute oxygen content and only slightly decreases the total amount of oxygen bound as oxides. K. E. Höner and S. Baliktay [22] examined the reaction rate of SiO_2 reduction by carbon inside Fe-C-Si melts. They found that equilibrium is reached after 2 to 3 hours at 1550 to 1500 °C and after 4.5 hours at 1450 °C, concluding that the reduction of silicon dioxide by carbon proceeds slowly inside the liquid metal. However, in the present experiments it takes only 4 to 6 minutes to cool down from 1500 °C to 1450 °C. It explains why, in this instance, silicon controls oxygen activity above the equilibrium temperature T_G.

Of course, above T_G, the amount of silicon dioxide formed will remain low because it is reduced by carbon from the melt. The CO remains in solution in the melt — possibly in supersaturation — because the formation of bubbles requires a lot of pressure in order to overcome the combination of the melt surface tension, the ambient pressure and the metallostatic pressure. Hence, CO bubbles will probably form close to the melt surface because here metallostatic pressure is minimal. On the other hand, the sensor measures oxygen activity below the melt surface (about 8 cm). The reduction of a silicon dioxide layer on the melt surface by carbon represents very favorable conditions because here no bubble formation is required as the gaseous CO can readily diffuse into the air. Consequently, the activity of oxygen well below the melt surface may be different from the melt close to the surface where CO bubbles nucleate.

Once the temperature drops below the equilibrium temperature for reduction of SiO_2 by carbon (T_G), measured oxygen activity seems to remain constant (Figure 2). In the original paper [9] this was explained as follows. As temperature decreases, more silicon dioxide forms because the equilibrium of Equality (7) shifts. Below the temperature T_G, silicon dioxide can no longer be reduced by carbon and its amount in the melt will increase. This raises the fraction of SiO_2 in the complex solid compounds and hence also increases the SiO_2 activity. The net effect is that measured oxygen activity remains nearly constant until finally the activity becomes (close to) one. Here measured and theoretical oxygen activity become (nearly) equal. Unfortunately, temperature has dropped (1330 °C) which makes the response of the sensor

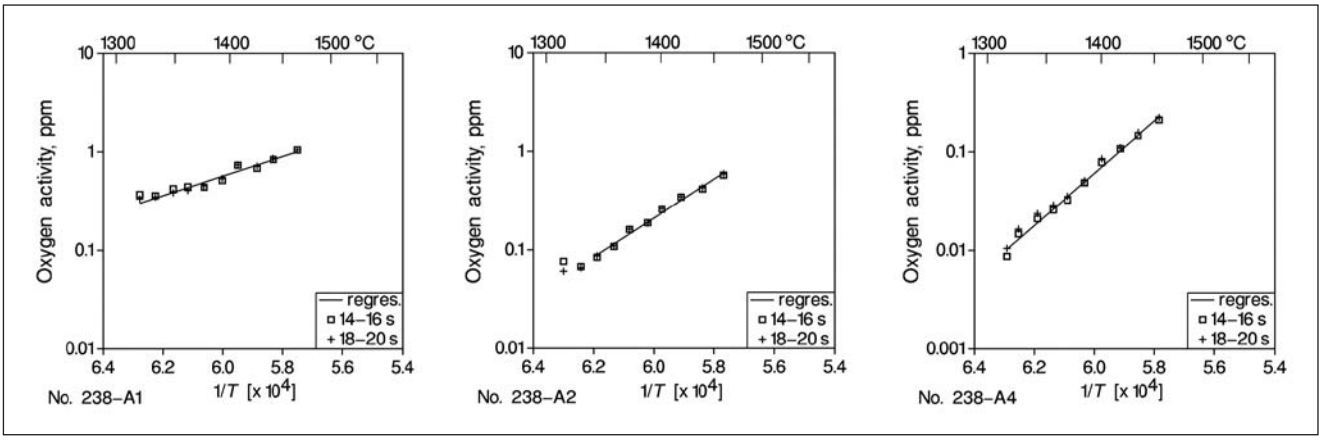

Figure 5: Oxygen activity as a function of temperature for 0.12 % Ti [9], after addition of 0.1 % NiMg (A1), 0.2 % NiMg (A2) and 0.4 % NiMg (A4) (results obtained with the old version of the Foundry Sensor)

slow. For this reason, no measurements at lower temperatures have been carried out.

3.4 Relation between oxygen activity and other parameters

Magnesium simultaneously reacts with oxygen and sulfur present in the melt. From a chemical point of view, these reactions are well defined by chemical equilibria. Consequently, one expects to find clear relationships between oxygen activity and sulfur or magnesium. Unfortunately, this is not the case. **Figure 3** shows oxygen activity versus the residual magnesium content for some selected melts with different sulfur content. Oxygen activity is the average value for 1420 °C obtained by regression analysis; magnesium and sulfur content have been interpolated between chemical analysis results just above and below 1420 °C. This figure shows the same behavior for every melt but no unique relation. The lack of a unique correlation results from the fact that the initial oxygen activity before magnesium addition differs from melt to melt. In each melt, small additions of magnesium (about 0.006 %) have no effect on oxygen activity because first of all available oxides in the melt (SiO_2, FeO, MnO) are reduced which has no effect on oxygen in solution. Higher magnesium contents decrease oxygen activity in all melts at a similar rate. Once oxygen activity has dropped to 0.12 ppm, further addition of magnesium has much less effect which is in line with the theory as given by equation (9). It is shown in Figure 3 for an activity of MgO equal to 0.3.

Similarly, X_s = S % - 1.32 Mg % has been used to look for a possible relationship (**Figure 4**). The parameter X_s has been employed in the past to plot the transition of graphite structures from spheroidal to compacted and lamellar [23]. X_s represents sulfur content minus the stoichiometric quantity for MgS formation. The idea is that this amount of Mg is required to neutralize sulfur and that the extra magnesium would uniquely determine graphite shape, or possibly in the present case, also oxygen activity. Again, every melt shows a similar relationship of decreasing oxygen activity with lower X_s values. However, the set of all experimental data lacks a unique relationship. There are several reasons to explain this fact. First, every melt contains a variable amount of oxides. E. Hofmann and G. Wolf [1] showed that the same melting procedure and charge materials can produce quite different quantities of oxides. J. Müller and W. Siefer [24] noted that oxygen content in pig iron and inoculants may vary largely. C. Labreque e. a. [25] found high oxygen content and large variations (96 to 185 ppm) in Sorel iron. Also holding of the melt changes the oxides content [26]. Consequently, if we assume that silicon dioxide occurs as a solid mixture then the activity of SiO_2 will also be different. According to Equation (7), a change of the activity of SiO_2 directly modifies the activity of oxygen at a given temperature. This also explains why the oxygen activity measured in various melts, but with the same chemical composition, can be different at the same temperature. In his review paper, A. McLean [27] notes that the activities of oxides in steelmaking are not known. The oxides present in the melt are reduced by magnesium and this is not taken into account in X_s. Moreover, the magnesium content introduced in X_s is the residual amount obtained by spectrometry and is the sum of free magnesium in solution and combined magnesium in oxides and sulfides. What is needed in fact is the magnesium activity as x coordinate in Figure 4. H. Itofuji [28] came to these same conclusions earlier based on careful research.

The only clear relationship with oxygen activity that could be derived from the experimental data is with the slope of the logarithm of the oxygen activity which is the coefficient of $1/T$ in the regression equation (Equation (8)). Equations (7) and (9) show a distinct difference for this coefficient in case SiO_2 or MgO is formed. This is also clearly illustrated by the experiments (**Figure 5**). The slope of the curve increases as more magnesium is added to the melt. More experimental data are compiled in **Figure 6**. This Figure shows that the coefficient of $1/T$ changes gradually when oxygen activity decreases. The coefficient of $1/T$ is a parameter which is directly related to the magnesium activity. At low oxygen activity (about 0.1 ppm) the coefficient of $1/T$ is equal to the coefficient valid for MgO formation (Equation (9)). With increasing oxygen activity, the coefficient goes up to -1.30×10^4 at 0.75 ppm oxygen activity and remains constant for higher oxygen activities. The value is somewhat higher than expected for SiO_2 formation (-1.54×10^4, Equation (7)). This difference will be explained below.

3.5 Physical meaning of the coefficient of $1/T$

The coefficient of $1/T$ in Figure 6 (equation (8)) is according to Equations (5) to (6), equal to

$$\log a_O = coefficient \frac{1}{T} + C \quad (19)$$

with

$$coefficient = -\frac{\Delta H^0}{\ln(10) R}$$

The coefficient is proportional to the standard enthalpy change. For a reaction at constant pressure, the enthalpy change is equal to the heat evolved by a reaction. Exothermic reactions give a negative value for ΔH. Note that putting log a_0 on the left hand side in Equations (8) and (19), virtually reverses the reaction to the oxide decomposition, which explains the positive value for ΔH.

At low oxygen activities, Figure 6 gives on average, values equal to -2.57×10^4 which corresponds to the heat associated with MgO formation. It means that in these circumstances, all oxygen in solution in the melt which reacts to form an oxide, does this with magnesium. On the other hand, when no magnesium is present as a solute, the coefficient of $1/T$ is -1.30×10^4. This value should be compared with -1.54×10^4 for SiO_2 formation, -0.73×10^4 for FeO formation and -1.51×10^4 for MnO formation. Consequently, as more FeO forms instead of SiO_2, less heat is released and the coefficient of $1/T$ decreases in absolute value. Interpolation of the present data reveals that 30 percent FeO forms. K. Orths e. a. [19] found by experiment that the oxygen bound as FeO + MnO varies between 25 and 50 percent of the total oxygen content. This is in line with the present experimental value of on average, 30 percent FeO, however derived in a completely different experimental way. The possible variation of FeO between 25 and 50 percent (coefficient of $1/T$ -1.34×10^4 and -1.13×10^4 respectively) is reflected for the present experiments by the dispersion on the coefficient of $1/T$ in Figure 6 when magnesium is absent in the melt. When sufficient magnesium is present only MgO forms reducing the dispersion in Figure 6.

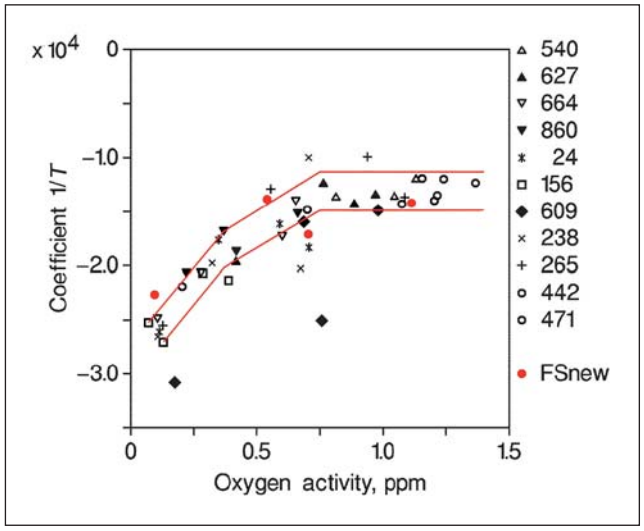

Figure 6: Coefficient of 1/T in Equation (8) versus oxygen activity at 1420 °C [9], FSnew refers to the new Foundry Sensor

This finding has an important practical consequence. The oxygen activity in a base melt (no magnesium or similar elements with high affinity for oxygen present) may vary because the oxygen in solution differs but also because the activity of the solid silicon dioxide can change. The latter is quite probable since the FeO-SiO_2 ratio can vary between relatively large bounds.

3.6 Recalculation procedure for oxygen activity

In order to compare measured oxygen activities, it is necessary to recalculate measured oxygen activities to a given, constant reference temperature. In the present paper 1420 °C has been chosen. However, the data provided in Table 2 and Figure 6 pertain to 1420 °C whereas values are needed at the measured temperature. To solve this problem, a simple iteration is applied which is explained here. Suppose we measure 0.36 ppm for the oxygen activity at 1390 °C. Since we do not known the slope valid at 1390 °C (i. e. the coefficient of $1/T$ in Equation (8) as shown in Figure 6 for 1420 °C) we simply take the slope for a_0 = 0.36 ppm at 1420 °C and recalculate using Equation (8):

$$\log a_O^{1420C} = \log a_O^{1390C} + coefficient\left(\frac{1}{1420+273} - \frac{1}{1390+273}\right) \quad (20)$$

which gives us 0.568 ppm at 1420 °C. In the second iteration we take the slope for a_0 = 0.568 ppm at 1420 °C. After four iterations we find 0.534 ppm which does not change during further iterations. As a conclusion, a_0 = 0.53 ppm at 1420 °C gives the correct slope (Table 2) which corresponds with an oxygen activity of 0.36 ppm at 1390 °C. Of course, at low (<0.12 ppm) or high (>0.75 ppm) oxygen activities, the slope is constant which gives us immediately the correct recalculated oxygen activity (after 1 iteration).

4 Differences between old and new foundry sensor

One of the authors (Frans Mampaey) and his colleagues at Sirris have carried out a large number of experiments using the first version of the Foundry Sensor. Considerable differences in the behavior of the old and new version of the oxygen activity sensor were noted. First of all, the equation — as supplied by the manufacturer — to calculate the oxygen activity from the measured emf and temperature is exactly the same for the old and new versions of the sensor. However, the shape of the emf curve as it occurs during the measurement differs. Numerous measurements at the author's research center showed that the emf curve of the old sensor frequently varied after the initial response (see for example the solid emf curve 1 in **Figure 7**). In order to compensate for this behavior, oxygen activity was calculated by averaging emf and temperauture values included within the time intervals of 14 to 16 s and between 18 to 20 s using dedicated data acquisition instrumentation. By contrast, the new sensor quickly produces a very stable emf signal (**Figure 8**). Consequently, all measurements using the new sensor have been obtained with instrumentation supplied by the probe manufacturer.

More importantly, the new sensor displays very high stability as a function of the bath temperature. As already explained before, theory predicts a linear relationship between the logarithm of the oxygen activity and the inverse

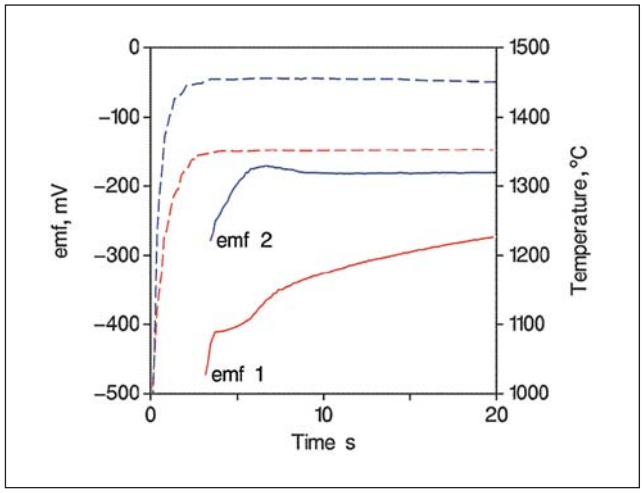

Figure 7: Example of emf and temperature output signals during measurement with the old oxygen activity sensor (red and blue lines refer to two different measurements)

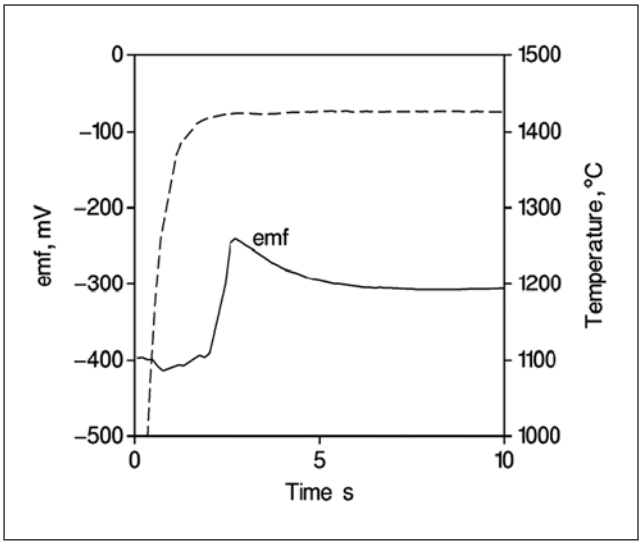

Figure 8: Typical signal produced by the new probe

of the absolute temperature (Equation (8)). The old sensor presented more dispersion especially at lower temperatures (**Figure 9**). **Figure 10** illustrates results for the new sensor, indicating excellent linearity over a large temperature interval both for gray and ductile iron. Again, the coefficient of $1/T$ differs depending on the presence of magnesium and is in line with the results published previously (Figure 6).

Finally, according to the manufacturer, the new sensor should be well suited to measure the very low oxygen activities typically for ductile iron. This was the main topic to be investigated by the present research.

5 Experimental procedure

The goal of the present experiments is to examine if a useful relation can be established between oxygen activity and various properties of ductile iron (tensile strength, yield strength, elongation, hardness) as well as the graphite and matrix structure.

In order to cover the complete range of ductile iron, the transition from spheroidal graphite to compacted graphite and occasionally also lamellar graphite has been examined.

Basically, oxygen activity is measured while holding a magnesium treated melt at constant temperature in the furnace. During holding, magnesium gradually evaporates resulting in changes to ductile iron properties. These changes are monitored by regularly pouring standard test bar molds.

Base ductile iron charges have been melted in an induction furnace of 300 kg. For ductile iron with a ferritic matrix, the charge (220 kg) consists entirely of Sorel iron. For ductile iron with a mixed ferritic-pearlitic matrix the same charge was deliberately kept in order minimize changes of the process variables. For these grades, the melt composition was adjusted using copper. Magnesium is added to each melt twice. The first treatment uses FeSiMg wire (7.5 % Mg) at about 1500 to 1520 °C. Once the magnesium reaction is over, the furnace is powered again in order to maintain a constant melt temperature in the furnace of about 1420 °C. At regular intervals of about 5 minutes, a standard Y-block (25 mm) is poured using a ladle of 20 kg liquid metal. During filling of the ladle, a 0.3 % addition of a proprietary zirconium-based inoculant (75 % Si, 2.5 % Ca, 1.4 % Al, 1.6 % Zr) is added in the stream. Specimens for chemical analysis are taken from the furnace using immersion samples (HEN SAF400). Maintaining the melt at constant temperature, gradually lowers the magnesium content. The regular pouring of Y-blocks continues until finally compacted or gray iron results. Depending on the initial melt composition, the transition from ductile to compacted graphite iron covers

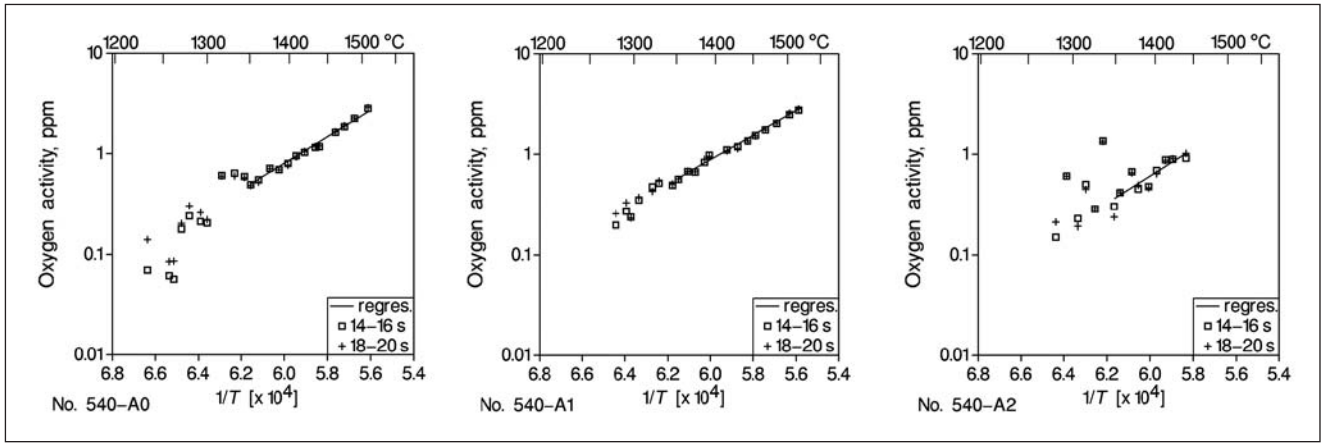

Figure 9: Oxygen activity as a function of temperature for 0.007 % S [9]: a) without Mg (A0), b) after addition of 0.1 % NiMg (A1) and c) 0.2 % NiMg (A2) (results obtained with the old version of the Foundry Sensor)

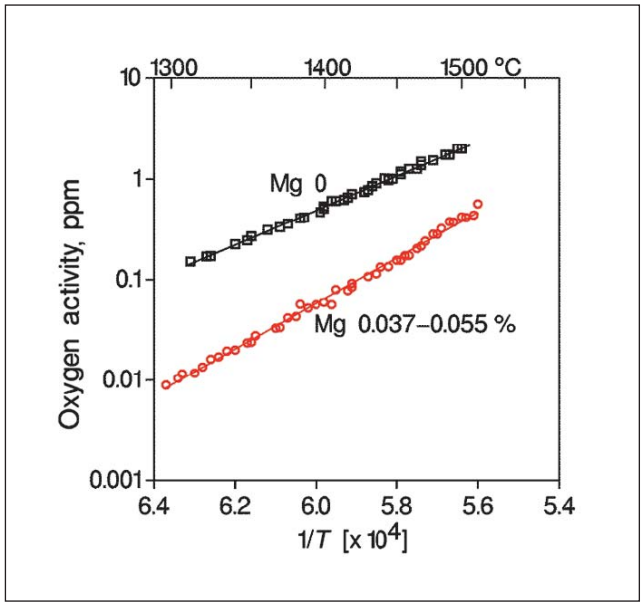

Figure 10: Oxygen activity measurements using the new Foundry Sensor, in melts with and without magnesium, at variable temperature

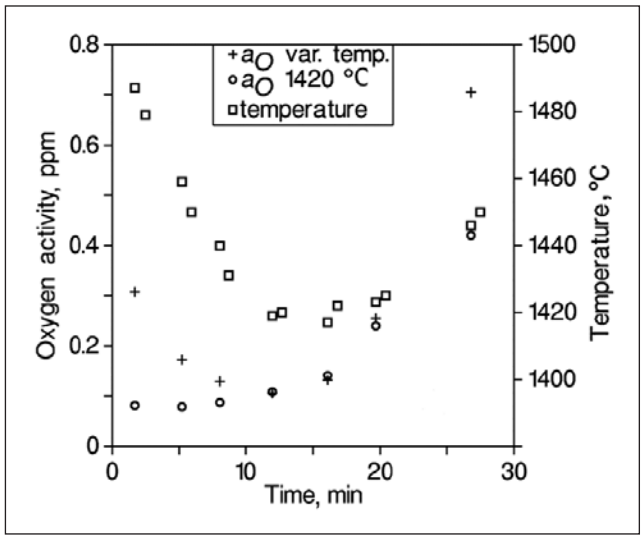

Figure 11: Oxygen activity as measured at the melt temperature and adjusted oxygen activity for 1420 °C; during holding residual Mg drops from 0.045 % (5 min) to 0.007 % (27 min)

about 35 minutes. In this way, about 7 Y-blocks are poured. Apart from the magnesium content, other elements vary only little during holding in the furnace. In the figures, time equal to zero corresponds to the end of the magnesium reaction in the furnace.

After the first series, 140 kg Sorel iron is added to the melt remaining in the furnace. After the Sorel iron, a second magnesium treatment using NiMg (15 %) follows. In this way, it is possible to keep the silicon content within the usual industrial range. In order to examine the whole magnesium range in ductile iron, a considerable amount of magnesium was added giving a relatively high initial residual magnesium content. Exactly the same procedure is maintained after the second magnesium addition as after the first treatment.

After cooling to room temperature, standard test bars (DIN-50125-B14) are machined from the Y-blocks. Mechanical testing is done according to the European Standard EN-10002-1, giving yield strength, ultimate tensile strength and elongation. A stress-strain curve is obtained using a video camera and real time computer analysis of the digitized pictures. Brinell hardness is measured as HBW 10/3000. After mechanical testing, a specimen for metallographic examination is taken from the test bar at about 5 to 8 mm distance from the crack. This procedure is the same for all graphite types, in ductile, compacted and gray iron. The normal procedure is a repetitive polishing and etching (5 times) before making the pictures. Magnification is 200× for the analysis of the graphite structure and 100× for the measurement of the ferrite content. Ferrite content is calculated as the average of 6 pictures, taken after nital etching (the sum of ferrite, pearlite and graphite is 100 percent). Four pictures are taken close to the edge, regularly spaced in the four directions of a compass, and two pictures in the center. After polishing, 10 photographs are taken of each specimen (tif format, 2088 × 1550 pixels). Each photograph is examined by image analysis and results are saved. Finally, average results for all 10 pictures are calculated. Particles with a size smaller than 10 pixels (3 µm) are not used for examination. Average results are pixel weighted unless otherwise mentioned. The average value F_a of a certain feature F is calculated by multiplying the value F_i for particle i with the number of pixels of this particle (W_i) using Equation (21).

$$F_a = \frac{\sum_n F_i W_i}{\sum_n W_i} \qquad (21)$$

This technique implies that the influence of small particles becomes less important.

Image analysis of graphite particles in cast iron uses a new method developed by one of the authors (Frans Mampaey). The contour of each particle is represented by a set of connected line segments. The mathematical description of the contour permits to calculate the length to thickness ratio of each particle. This feature is easy for human interpretation and should be the preferred method for all non-spherical objects like compacted graphite particles and graphite lamellae. The length to thickness calculation differs basically from current techniques, which rely on a comparison of particle features with those of a circular object. A detailed description of the method as well as its application to compacted graphite cast iron has been published before [29, 30]. All graphite particles are divided into 4 classes, based on the length to thickness ratio (**Table 1**). Class SG is considered grouping spheroidal graphite particles. Compacted graphite cast iron is generally defined to contain particles with length to thickness ratio between 2 and 10, this class is denoted by CG. During the research, it became clear that two additional

Table 1: Four classes used for graphite particle classification

Class name	Length to thickness ratio min	max	Graphite morphology
SG		2	spheroidal
CG	2	10	compacted
G10-20	10	20	
LG > 20	20		lamellar

classes instead of just one class were needed for particles with a length to thickness ratio larger than 10. These are denoted G10-20 for particles with a length to thickness ratio between 10 and 20, and LG > 20 for particles with a length to thickness ratio larger than 20. This last class (LG > 20) is generally considered as lamellar graphite. However, image analysis research has shown that this hypothesis is not entirely correct. In compacted graphite cast irons, vermicular particles with length to thickness ratios larger than 20 occasionally occur. The fraction (or percentage) of SG particles corresponds to the nodularity.

The oxygen activity sensor measures emf and temperature. For experiments carried out previously [31, 9] emf and temperature signals were captured from the vibrating lance signal output. Dedicated equipment and software stored emf and temperature data as a function of time during measurement. Using the original data curves, oxygen activity was calculated at fixed moments (10 and 20 s [31]) or averaged (14-16 s and 18-20 s [9]). The temperature was averaged between 10 and 20 s. Calculation of oxygen activity from emf and temperature was carried out using the equations supplied by the probe manufacturer. This method was employed because the old version of the sensor occasionally produced slowly but continuously varying emf output during measurement.

In the present research, a new version of the oxygen activity sensor combined with appropriate equipment of the probe manufacturer are used to measure the oxygen activity. The new sensor produces a very stable curve soon after immersing the probe. Hence, it became quickly obvious that this method provided optimal results.

In order to examine experimental results, the measured oxygen activities need to be compared. Because oxygen activity strongly varies with temperature, a constant reference temperature of 1420 °C has been chosen for comparison. This holding temperature has been chosen because it represents a suitable pouring temperature for ductile iron. Previous research has shown that the temperature correction for the oxygen activity is not constant but varies with oxygen activity (Figure 6). Figure 6 basically means that the temperature coefficient of the term $1/T$ in Equation (8) requires adjusting $\log(a_0)$ to a reference temperature, changes between lamellar graphite cast iron ($a_0 \geq 0.75$ ppm) and spheroidal graphite cast iron ($a_0 \leq 0.12$ ppm). In the present experiments, this procedure is only important in the transition zone of compacted graphite iron. Indeed, all ductile irons have the same temperature coefficient for $\log(a_0)$ correction which is equal to the theoretical value derived using standard chemical relations and chemical reaction data (Equation (9)). The numerical data for the conversion are listed in **Table 2**. The average slope of the logarithm of the oxygen activity as a function of $1/T$ depends on the oxygen activity at 1420 °C. Between 0.12 ppm and 0.75 ppm, the slope has been be linearly interpolated as a function of the oxygen activity.

Table 2: Average slope of the logarithm of the oxygen activity as a function of $1/T$; oxygen activities are valid for 1420 °C

Oxygen activity, ppm	Slope
<0.12	-2.57×10^4
0.3	-1.95×10^4
≥0.75	-1.30×10^4

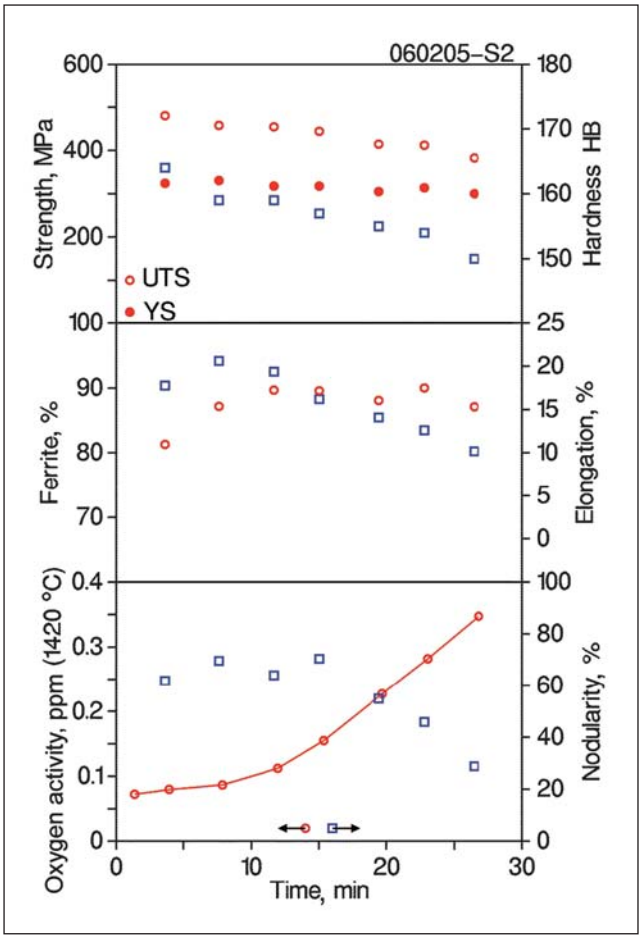

Figure 12: Oxygen activity (1420 °C), tensile strength (UTS), yield strength (YS), Brinell Hardness, elongation, ferrite content and nodularity during holding of melt 060205-S2. During holding residual Mg drops from 0.052 % (3.3 min) to 0.009 % (26 min). All square symbols pertain to the right hand y-axis.

6 Results

6.1 Ferritic ductile iron

The need to adjust measured oxygen activities to a constant reference temperature as explained above, may be illustrated by **Figure 11**. The Figure shows the measured oxygen activities without any correction, i. e. valid for the melt temperature. Just after magnesium addition by NiMg, the furnace temperature is relatively high. Because of this high bath temperature, the measured oxygen activities are high too, and subsequently drop to a minimum after 12 min before increasing again.

There is little we can do using this unadjusted data. Much better and more useful information is provided by the adjusted oxygen activities valid for the constant reference temperature of 1420 °C. Now it becomes clear that oxygen activity increases as the magnesium in the melt decreases. In the remainder of the paper, only converted oxygen activity data will be plotted.

Figure 12 shows how oxygen activity, tensile strength, yield strength, hardness, elongation, ferrite content and nodularity change while holding melt 060205-S2 in the furnace. The chemical analysis for all melts can be found in **Table 3**. Yield strength varies little, tensile strength decreas-

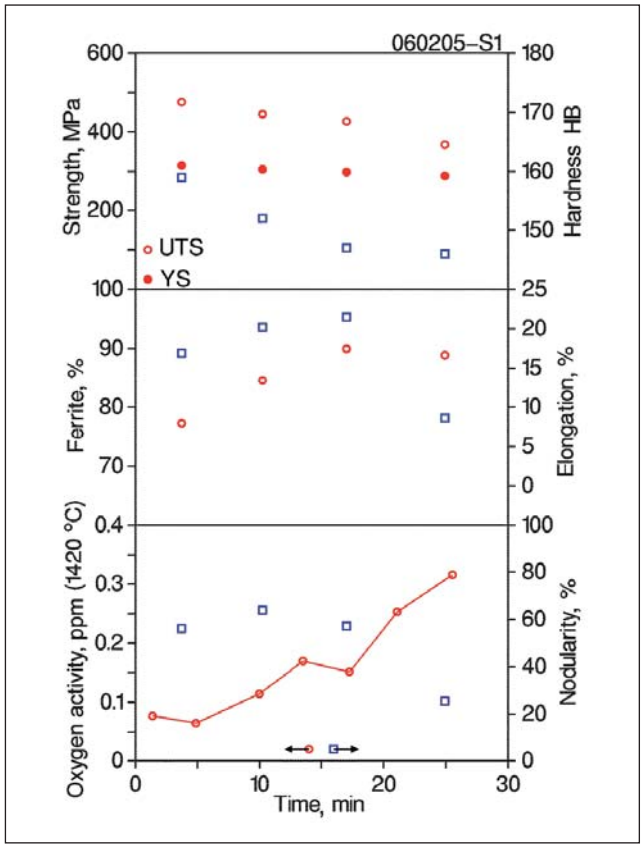

Figure 13: Oxygen activity (1420 °C), tensile strength (UTS), yield strength (YS), Brinell Hardness, elongation, ferrite content and nodularity during holding of melt 060205-S1

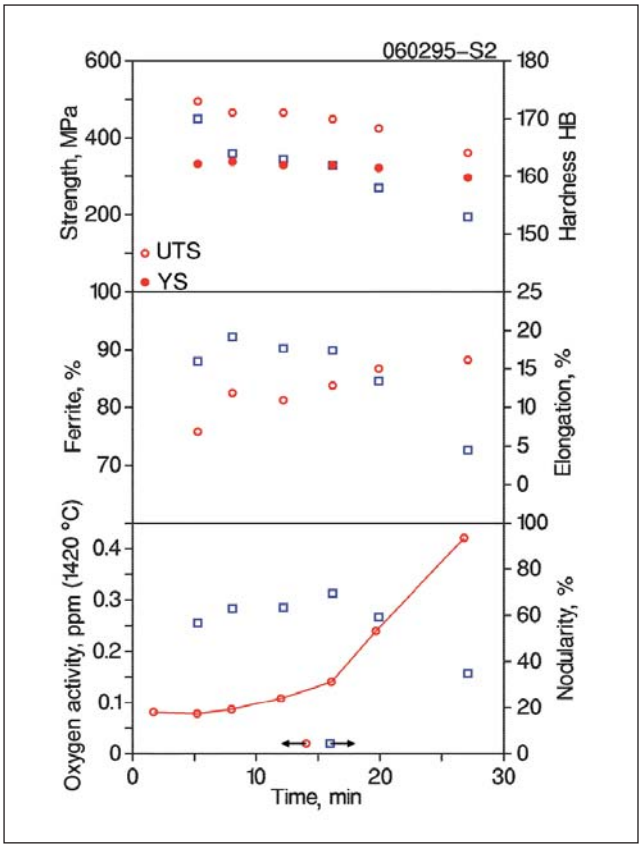

Figure 15: Oxygen activity (1420 °C), tensile strength (UTS), yield strength (YS), Brinell Hardness, elongation, ferrite content and nodularity during holding of melt 060295-S2

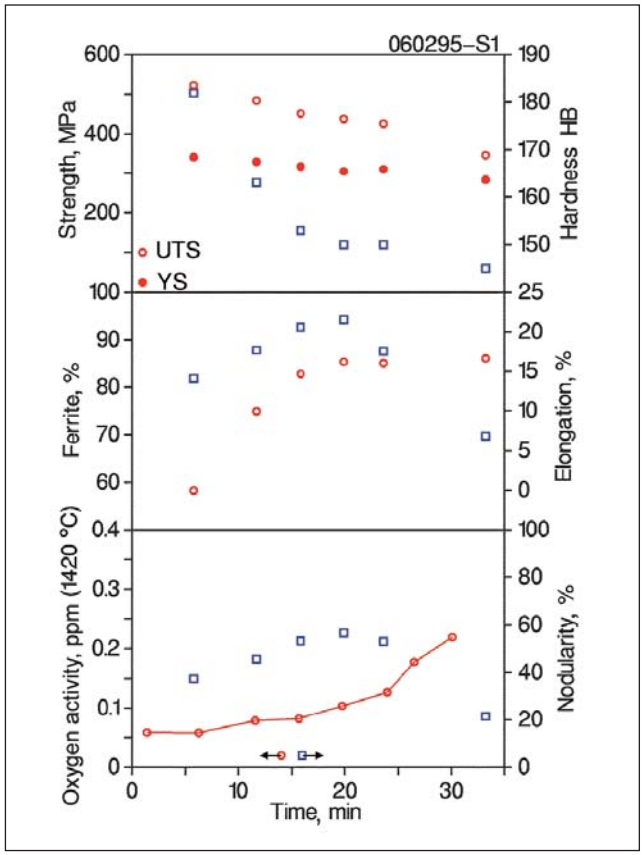

Figure 14: Oxygen activity (1420 °C), tensile strength (UTS), yield strength (YS), Brinell Hardness, elongation, ferrite content and nodularity during holding of melt 060295-S1

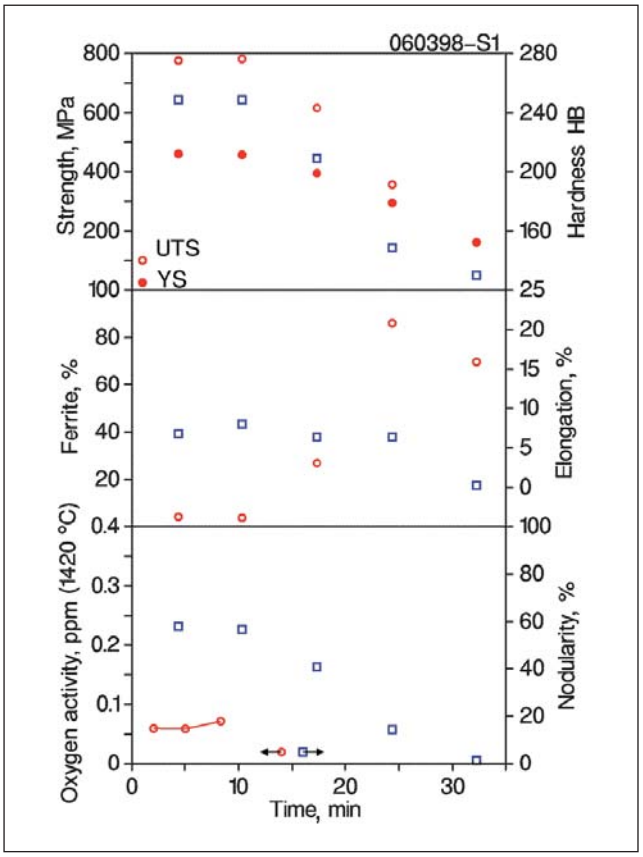

Figure 16: Oxygen activity (1420 °C), tensile strength (UTS), yield strength (YS), Brinell Hardness, elongation, ferrite content and nodularity during holding of melt 060398-S1

es more however, for elongation, a maximal appears. Figure 12 also shows ferrite content and nodularity (equal to SG). Most interesting information is provided by elongation, ferrite content and nodularity. Of course, for a given composition, elongation increases with higher ferrite content and nodularity. Results for all other heats of ferritic ductile iron are shown in **Figures 13** to **15**.

Figures 12 to 15 provide a lot of experimental information. First of all, the physical meaning contained in the figures should become clear. When the magnesium in solution becomes too low (for example in Figure 12 after 15 minutes) — or equivalently when oxygen activity increases — compacted graphite forms. Increasingly more compacted graphite particles in turn lowers the elongation. This phenomenon was also shown in a previous publication [31].

Ferrite content in ductile iron increases with oxygen activity. The result is quite remarkable but in line with previous experiments carried out by the author (not published). Note that ferrite forms at about 720 °C as a result of a solid state transformation whereas oxygen activity is measured in the liquid state. However, it is quite acceptable that low oxygen activity in the liquid will be in line with low activities in solid too. The relation between oxygen activity and ferrite content is not known today because a reliable oxygen activity measurement has not been available. All heats for ferritic ductile iron indicate that elongation becomes maximal when both ferrite content and nodularity are optimal. It allows us to examine if oxygen activity can be used to predict optimal conditions when producing ferritic ductile iron and to assess the reproducibility. **Table 4** lists the oxygen activity which corresponds to maximal elongation for all series.

All three experiments show that elongation becomes maximal — and mechanical properties optimal — at nearly the same value of the oxygen activity. This value corresponds to a "bending" point in the oxygen activity versus time curve. Below this value, oxygen activity slowly rises while above the value the oxygen activity increases faster. At the "optimal" oxygen activity, both ferrite and nodularity are high. At higher oxygen activity (or equivalently lower free magnesium) compacted graphite formation is favored which decreases elongation.

Table 4 shows that for the present case residual magnesium content is not a reliable parameter to determine the optimal condition. Residual magnesium content is the sum of magnesium in solution (corresponding to magnesium activity) and magnesium bound as a compound (e. g. as oxide, sulfide or in more complicated compounds). The melts with high initial magnesium content (series 1 with wire treatment) present less residual magnesium content at the optimal composition because sulfur has been eliminated mostly during holding.

Table 3: Chemical analysis for all heats

	Chemical element, mass percent						
No.	C	Si	Mn	S	Cu	Ni	Mg max
060205-S1	3.76	2.32	0.031	0.003	0.027	0.072	0.072
060205-S2	3.68	2.21	0.03	0.003	0.027	0.69	0.052
060295-S1	3.64	2.60	0.032	0.003	0.029	0.078	0.089
060295-S2	3.55	2.54	0.026	0.003	0.029	0.729	0.051
060398-S1	3.6	2.60	0.027	0.001	0.51	0.08	0.071
060398-S2	3.44	2.49	0.025	0.009	0.50	0.69	0.044
060426-S1	3.61	2.67	0.027	0.002	0.42	0.077	0.085
060426-S2	3.51	2.44	0.024	0.008	0.43	0.711	0.042

All heats: P 0.011-0.014; Cr 0.035-0.071; Mo ≤ 0.011; V 0.019-0.036; Al 0.008-0.024 (mass percent)

Table 4: Oxygen activity and maximal elongation for ferritic ductile iron

No.	Time, min	Elongation, %	Oxygen Activity, ppm	Mg res., %
060205 Series 1	17.03	21.5		0.024
060205 Series 2	7.6	20.6	0.09	0.036
060295 Series 1	19.9	21.6	0.10	0.025
060295 Series 2	8.0	19.2	0.09	0.042

6.2 Pearlitic ductile iron

In the second series, ductile iron with a mainly pearlitic composition was envisaged, while deliberately keeping changes in processing variables minimal. To this extent, the charge consisting of Sorel iron remained unchanged so that only the addition of a pearlite stabilizing element would differ. Copper was chosen to adjust the pearlite fraction in the matrix. All results are presented in **Figures 16** and **17**. Although few oxygen activities have been obtained for experiment 060398-S1, the other experimental data are shown because they confirm the results of experiment 060398-S2. In this series, ductile iron with excellent properties has been poured. While strength data meet EN-GJS-600-3 requirements, the elongation of 7 percent of EN-GJS-500-7 is met.

Figure 17 illustrates what happens when oxygen activity increases as a result of the drop of free magnesium content in the iron. Initially, the quality of the nodular graphite structure increases. This is illustrated by the image analysis data. The nodularity (i. e. the fraction of true nodular graph-ite, here with length to thickness ratio <2) becomes maximal (after 8.5 minutes in case of the experiment 060398 — series 2). The optimal point corresponds to the moment where the oxygen activity starts to rise faster. Ferrite content is slightly higher as compared to the initial values after nodulization. From this moment on, the further (faster) rise of the oxygen activity is accompanied by a decrease in the quality of the nodular graphite structure and by a pronounced increase of the ferrite content. Here, free magnesium content becomes too low resulting in rising activities of oxygen and sulfur in the melt. The practical consequence is the formation of increasing fractions of compacted graphite accompanied by a decrease in ultimate tensile strength and yield strength. The effect on elongation is more complicated. Higher oxygen ac-

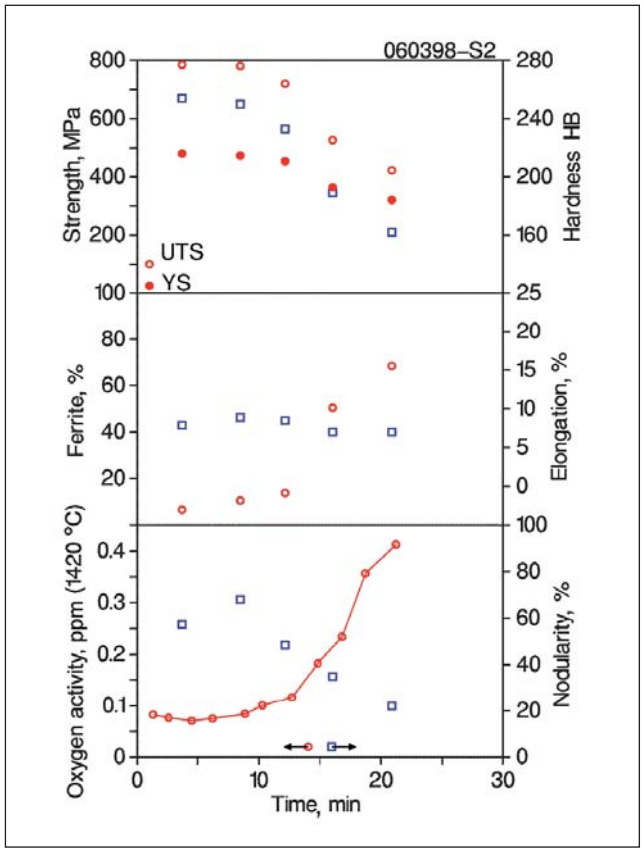

Figure 17: Oxygen activity (1420 °C), tensile strength (UTS), yield strength (YS), Brinell Hardness, elongation, ferrite content and nodularity during holding of melt 060398-S2

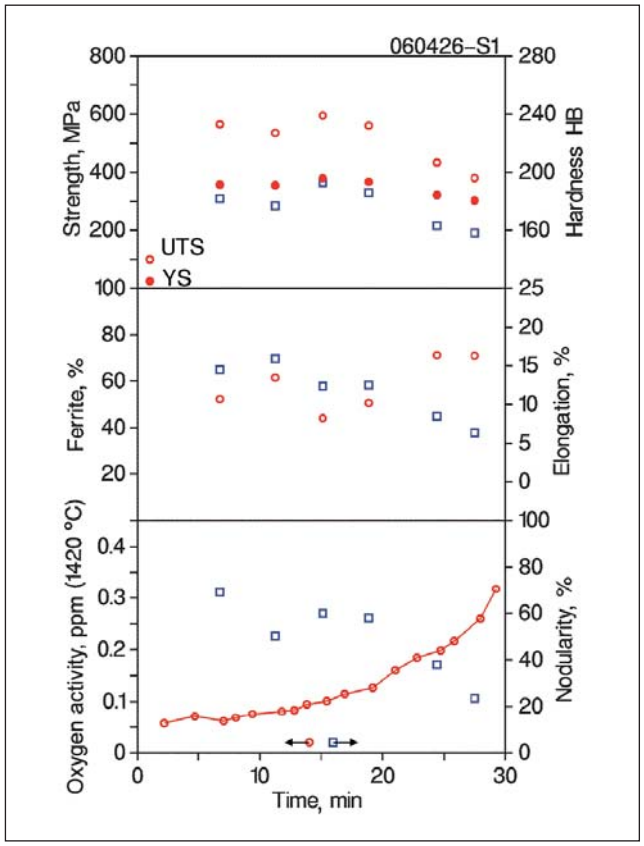

Figure 18: Oxygen activity (1420 °C), tensile strength (UTS), yield strength (YS), Brinell Hardness, elongation, ferrite content and nodularity during holding of melt 060426-S1

tivity simultaneously raises ferrite content and the fraction of compacted graphite particles, which on average also increase in size. Both factors have an opposite effect on elongation: more ferrite increases elongation while more compacted graphite decreases elongation. The simultaneous effect of a larger ferrite content and more compacted graphite, on elongation may be complicated. Summarizing, in the present experiment we start with a mainly pearlitic ductile iron which gradually obtains maximal properties with high pearlite content, optimal elongation and nodularity. A further rise of oxygen activity finally results in a ferritic compacted graphite cast iron with excellent elongation.

Table 5 lists the oxygen activity corresponding to maximal elongation and optimal graphite structure. It is the value equivalent to a "bending" point in the oxygen activity versus time curve. Below this value, oxygen activity slowly rises while above this value oxygen activity increases faster. Here, residual magnesium content is relatively constant and at the optimal condition.

6.3 Ferritic-pearlitic ductile iron

In this series, slightly less copper has been added in order to lower the pearlite fraction of the matrix (060398 Cu 0.5 % — 060426 Cu 0.42 %). It increases the ferrite content of the matrix from less than 10 percent to about 40 percent. Results are summarized in **Figures 18** and **19**. The minimal mechanical properties of the standard EN-GJS-500-7 are easily met within the nodular range, and even in the range where compacted graphite particles appear (nodularity about 50 percent).

The general trend in all the Figures gives a ferrite content which is relatively stable as long as the graphite has a good nodular structure. Once the nodularity starts to lower, ferrite content goes up very fast.

Finding the value of the oxygen activity which corresponds to maximal elongation proved to be more difficult for the series 060426. It is rather easy to find the optimal value for the ferritic irons probably because elongation is mainly determined by nodularity. As already mentioned, nodularity and ferrite content adversely influence elongation. However, the start of nodular graphite deterioration can be easily noticed using oxygen activity measurements (preferably corrected to constant reference temperature of 1420 °C). This start corresponds to the moment when oxygen activity starts to rise more quickly (**Table 6**). It is exactly the same as in the case of the other ductile iron heats. There too, residual magnesium content is relatively constant at the optimal condition.

It is interesting to examine the fading of magnesium during holding in both series (**Figure 20**). In series 1, Mg content of the melt decreased continuously (exponentially) but in series 2 there was a discontinuity evident at 11 min. Before this moment, magnesium content dropped very slowly. This was due to the power supply in the furnace. Treatment with NiMg (060426-S2) lowers the temperature in the furnace little. As a result no power was supplied to the furnace during the first 11 minutes. The melt in the furnace was calm and in these circumstances magnesium fades very slowly. Once the power is turned on to keep the metal in the furnace at constant temperature, stirring of the liquid begins and magnesium fade increases substantially. Exactly the same phenomenon has been noticed during the other experiment (060398). It explains why properties of the samples in the second series ini-

tially vary very little as long as the melt in the furnace remains calm (i. e. without power supply). The most important conclusion from this behavior pertains to the use of time as a production control factor. Magnesium fade depends on many factors, in the present case from the intensity and duration of power supply. Hence, magnesium content may decrease irregularly and not reproducibly as a function of time. Measurement of oxygen activity gives values which are reproducible and independent of the rate of magnesium fade.

Very importantly, all measured oxygen activity data — as well as the recalculated data corresponding to 1420 °C — show very little dispersion and closely follow the average curve during each experiment, proving two things. First of all, the measured data are stable and very reproducible and secondly, the correction procedure to recalculate all data to 1420 °C, is accurate.

7 Relation between examined properties and oxygen activity

The previous Figures revealed how oxygen activity and various properties change with time after nodulization. Oxygen activity varies slowly till about 0.1 ppm but afterwards it increases much faster. This behavior is in line with the expected theoretical behavior shown in Figure 1. However, as shown in Figure 20, magnesium fade — and because of its relation with oxygen, also oxygen activity (Equations (9) to (10)) — may be discontinuous as a function of time. Consequently, all properties examined have been plotted as a function of the oxygen activity. Because the relative time of each oxygen activity measurement as counted from the moment of the pouring of the keel blocks differs, some data should be interpolated. In the present research, oxygen activity data has been linearly interpolated to the moment of pouring the keel blocks. This procedure produces more accurate results than the use of a regression equation for oxygen activity as a function of time, which may be discontinuous as explained above.

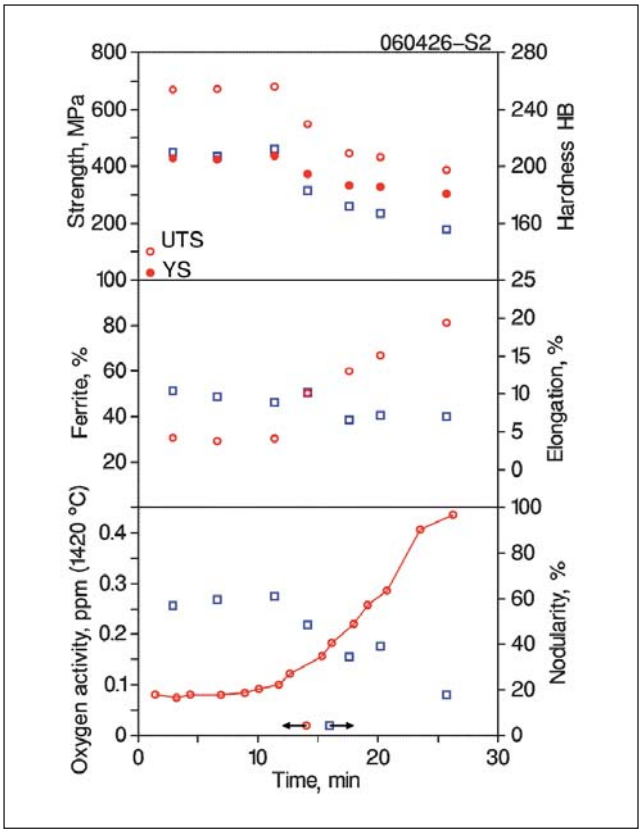

Figure 19: Oxygen activity (1420 °C), tensile strength (UTS), yield strength (YS), Brinell Hardness, elongation, ferrite content and nodularity during holding of melt 060426-S2

7.1 Nodularity

Figures 21 and **22** show nodularity as a function of the oxygen activity for irons with a ferritic and mixed ferritic-pearlitic matrix respectively. For ferritic irons, a maximal nodularity occurs for an oxygen activity between 0.10 and 0.12 ppm. When oxygen activity drops below 0.10 ppm, nodularity diminishes which is in line with the well-known foundry experience that too high magnesium content adversely influences nod-ularity. For iron with pearlite in the matrix, although less obvious, the optimal oxygen activity content seems to be the same. Once the oxygen activity becomes higher than the optimal value, nodularity quickly drops due to the presence of increasing amounts of vermicular graphite. Irons with compacted graphite containing nickel show a higher nodularity than iron without nickel at the same oxygen activity. Nodularity between 20 to 30 percent corresponding to compacted graphite cast iron, occurs for oxygen activities between 0.25 to 0.30 ppm in irons without nickel. If nickel is present, in these experiments because of NiMg treatment, nodularity between 20 to 30 percent occurs for oxygen activities above 0.35 ppm. Because of the limited number of experiments in the compacted graphite iron range, this data should be considered with some restraint.

7.2 Ferrite

In ferritic ductile iron (**Figure 23**) ferrite content raises quickly till about 0.12 ppm oxygen activity. If the matrix is not yet completely ferritic, a further rise in oxygen activities

Table 5: Oxygen activity and maximal elongation for pearlitic ductile iron

No.	Time, min	Elongation, %	Oxygen Activity, ppm	Mg res., %
060398 Series 1	10.3	8.0		0.038
060398 Series 2	8.5	8.9	0.08	0.042

Table 6: Oxygen activity and maximal elongation for ferritic-pearlitic ductile iron

No.	Time, min	Elongation, %	Oxygen Activity, ppm	Mg res., %
060426 Series 1	11.2	15.9	0.08	0.039
060426 Series 2	8.0	10.4	0.08	(0.042)

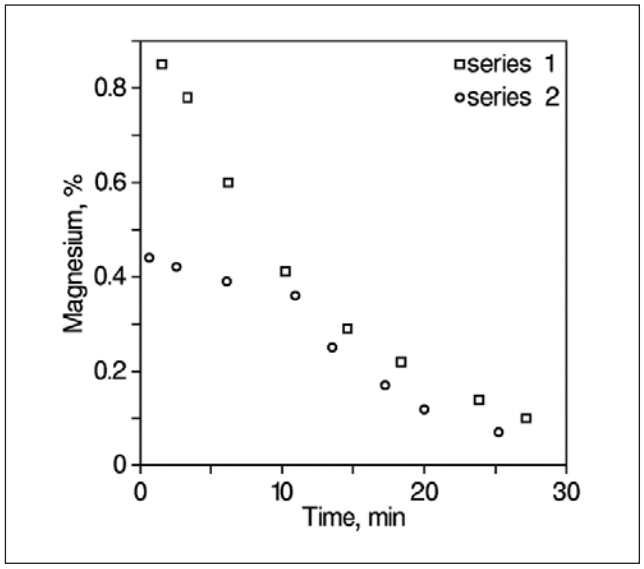

Figure 20: Residual magnesium content as a function of time during holding of melt 060426 S1 and S2

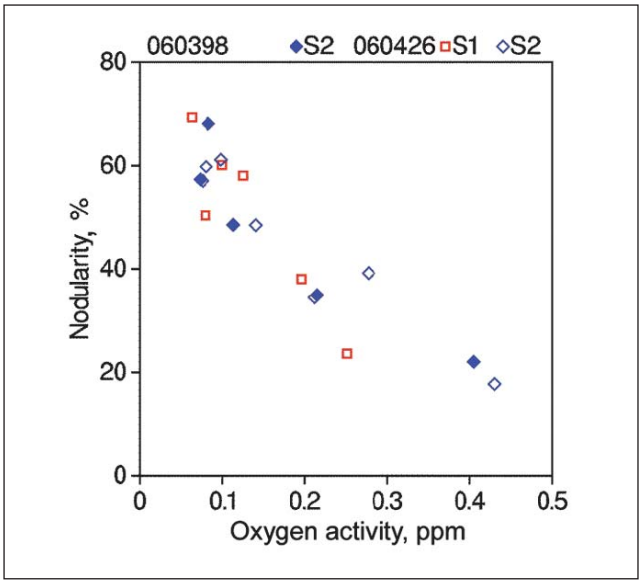

Figure 22: Nodularity versus oxygen activity for ductile iron with mixed ferritic-pearlitic matrix

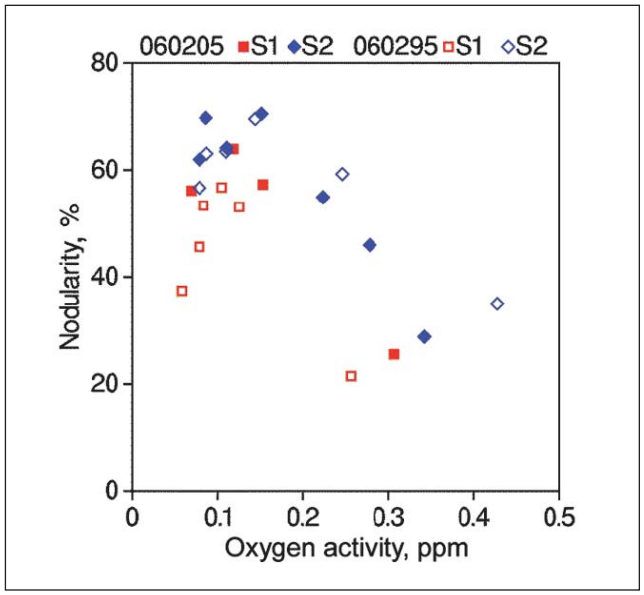

Figure 21: Nodularity versus oxygen activity for ferritic ductile iron; all S2 heats contain about 0.7 percent nickel

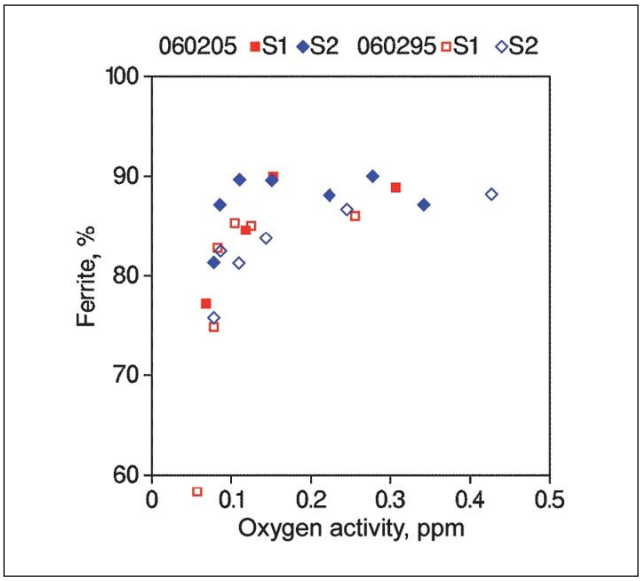

Figure 23: Ferrite content as a function of oxygen activity for ferritic ductile iron; the sum of ferrite, pearlite and graphite is 100 percent

removes pearlite much slower. In irons with less ferrite in the ductile iron matrix (**Figure 24**), ferrite content increases continuously with higher oxygen activity. The increase is larger when the initial ferrite content at low oxygen activity is smaller. All ductile irons with 50 to 90 percent pearlite finally transform to compacted graphite irons with 70 to 80 percent ferrite in the present experimental conditions where only copper has been added to promote pearlite.

7.3 Strength

In ferritic ductile irons (**Figures 25** and **26**) yield strength decreases very little with increasing oxygen activity. However, tensile strength drops more when oxygen activity goes up. In higher strength ductile irons, having more pearlite in their matrix, both yield strength and tensile strength decrease when oxygen activity increases (**Figure 27**). However, the drop in strength is more pronounced for the tensile strength. In all cases (ferritic and pearlitic) irons containing no nickel loose strength somewhat faster than nickel alloyed ones. Nickel containing irons have somewhat higher nodularity than nickel free irons at the same oxygen activity.

7.4 Elongation

In ferritic ductile irons, elongation seems to be maximal for an oxygen activity of 0.9 to 0.10 ppm (**Figure 28**). At lower oxygen activity, elongation is somewhat smaller probably because of lower nodularity. Once oxygen activity exceeds the optimal value, elongation steadily drops. For ductile irons with pearlite in the matrix and lower intrinsic elongation, no optimal value was noted (**Figure 29**). Because of the lower initial elongation, the drop is smaller too. Moreover, since all compositions finally end as compacted graphite iron with a predominant ferritic matrix, the final elongation does not differ so much (5 to 7 percent).

7.5 Hardness

In all irons examined, hardness decreases with rising oxygen activity (**Figures 30** to **31**). The drop is most pronounced in the lower oxygen activity range. For ferritic compositions, the presence of nickel is accompanied by somewhat higher hardness (Figure 30).

Hardness is quite important for castings, which have to be machined. A low and constant hardness is very favorable for machining. The lower the hardness, the longer the lifetime of the cutting tool. Because hardness depends on the amount of pearlite in the matrix (as well as on the fineness of the pearlite), more pearlite decreases machinability. The present results show that within the range of ductile iron, the compositions with the optimal oxygen activity (for nodularity and elongation) also have the lowest hardness.

7.6 Grain count

In cast iron literature, several authors have mentioned that a minimal amount of oxygen is needed in order to obtain efficient inoculation (e. g. S. Lekakh 2003 [32], T. Skaland [33]). In the present experiments, once the magnesium treatment is finished, oxygen activity — or equivalently oxygen in solution in the iron — rises in time. In order to examine a possible effect of oxygen activity on inoculation treatment, the number of graphite particles counted using image analysis were analyzed for all experiments (**Figures 32** to **33**). Inoculation was carried out during filling of the ladle with 0.3 % of a zirconium containing inoculant. Because this was a manual inoculation treatment, the addition rate of the inoculant was not constant and the inoculant did not dissolve at the same rate in the melt. This may have resulted in some dispersion on the particle counts so that the average trend is important rather than individual points.

In ductile iron, each nodule represents a graphite particle nucleated on one heterogeneous substrate. When nodularity decreases, graphite appendices appear on the initial graph-ite spheroids. Here, one vermicular particle will probably result from one heterogeneous nucleus. However, in the compacted graphite iron range, a “eutectic cell” grown from only one heterogeneous substrate may result in a three dimensional structure composed of many trunks. In this case several individual vermicular particles will belong to only one “eutectic cell”. In the case of gray iron even many more lamellae compose one eutectic cell.

In order to examine a possible influence of oxygen activity on nodule count, only particle counts for oxygen activities below 0.15 ppm have been considered. These circumstances correspond to true ductile irons. For each series, a linear regression analysis has been carried out. The average of the seven series shows that nodule count increases with 128 particles (per mm^2) when the oxygen activity rises with 0.1 ppm. For an average nodule count of 300 per mm^2, this corresponds to a substantial increase of 42 percent per 0.1 ppm oxygen activity rise. Certainly, one of the areas in cast iron that has received major research interest in the past has been inoculation. Inoculation results often show large dispersion even within one research. Frequently, considerable differences occurred in the results for similar research carried out by different groups. If we consider the large effect of oxygen activity on inoculation, it could explain part of the differences evident between published research results. Oxy-

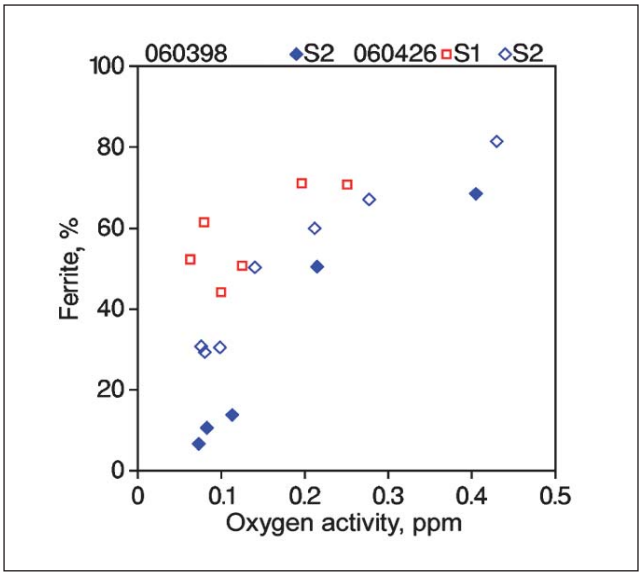

Figure 24: Ferrite content as a function of oxygen activity for ductile iron with mixed ferritic-pearlitic matrix

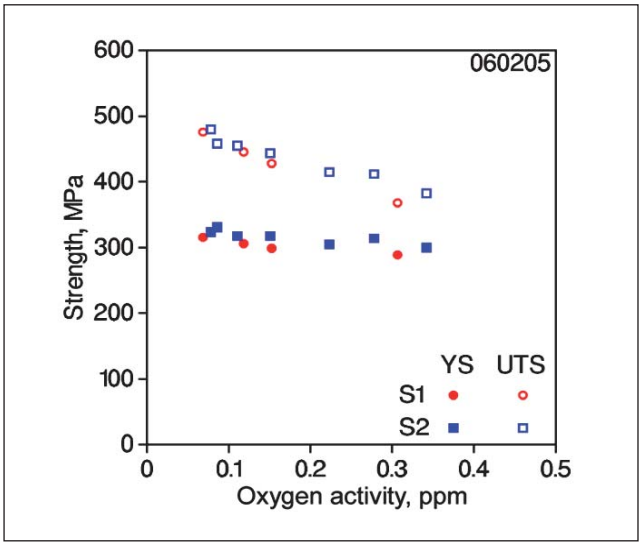

Figure 25: Change of yield strength and tensile strength with oxygen activity in ferritic ductile iron

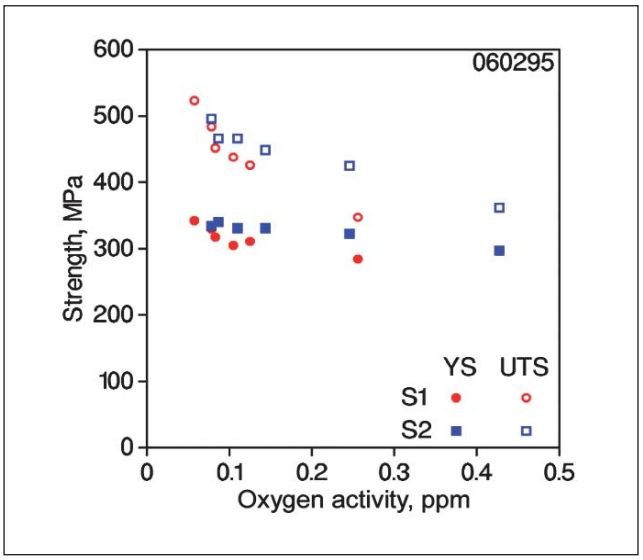

Figure 26: Change of yield strength and tensile strength with oxygen activity in ferritic ductile iron

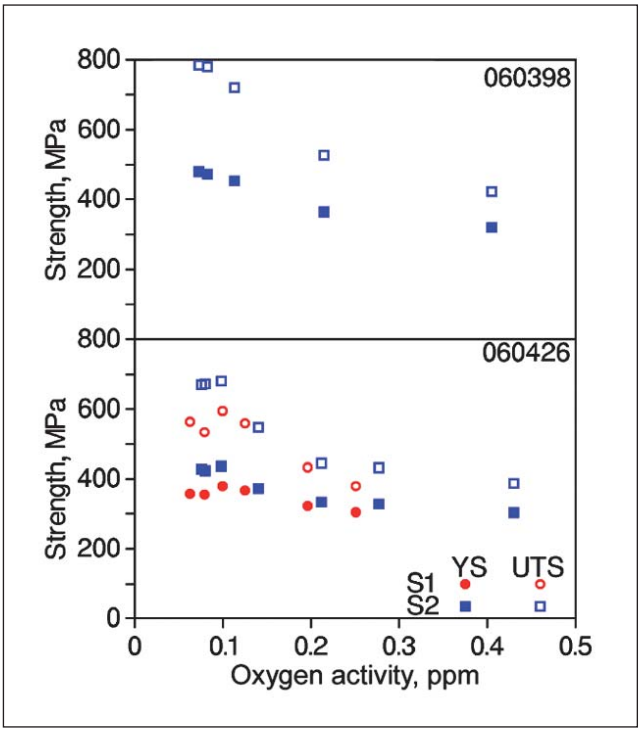

Figure 27: Change of yield strength and tensile strength with oxygen activity in ductile irons with a mixed matrix

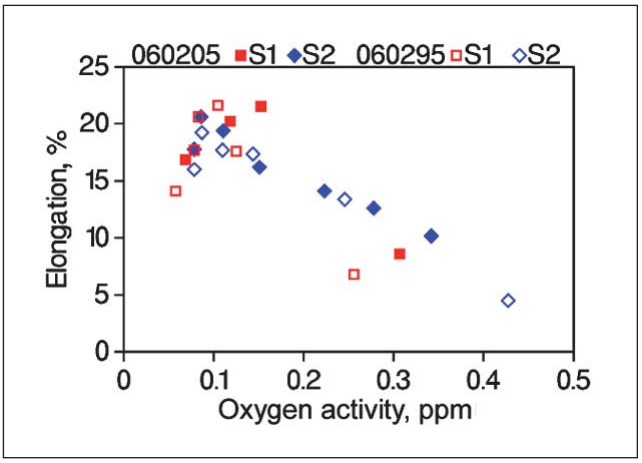

Figure 28: Variation of elongation with oxygen activity for ferritic ductile iron

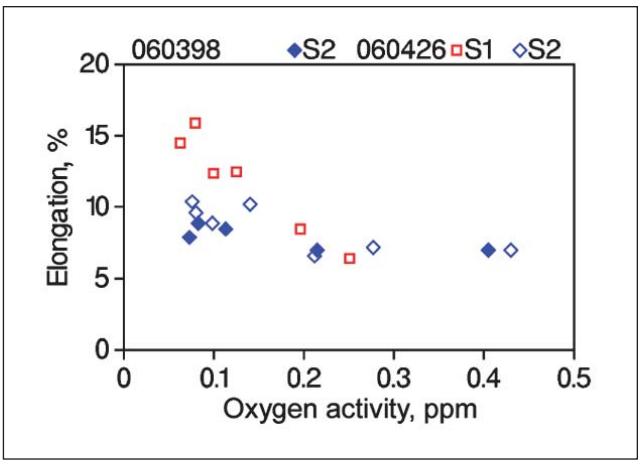

Figure 29: Variation of elongation with oxygen activity for ductile iron with mixed ferritic-pearlitic matrix

gen activity was indeed a parameter which had not been measured in the past during such experiments.

8 Conclusions

- During all experiments carried out, stable and reproducible oxygen activities have been measured. Since all oxygen activities have been recalculated to a constant reference temperature of 1420 °C, one can conclude that the conversion factor (i. e. the temperature coefficient of the oxygen activity) is reliable too. Recalculation of measured oxygen activities to a constant reference temperature is a prerequisite if ductile iron process control is envisaged.
- Optimal mechanical properties in ductile iron are obtained for a well-defined oxygen activity (0.09 to 0.10 ppm at 1420 °C). It is the result of high ferrite content and high nodularity occurring simultaneously. Residual magnesium is not a reliable parameter to assess the optimal melt condition.
- In ductile irons containing pearlite, ferrite content increases substantially once oxygen activity becomes higher than the optimal value. Compacted graphite cast irons having the same base composition as ductile iron (except magnesium) contain much more ferrite.
- Optimal oxygen activity corresponds to a “discontinuity” in the oxygen activity change. Below this value oxygen activity varies slowly, above this value, it increases much faster as a function of time.
- Within the ductile iron range, graphite particle count increases substantially with rising oxygen activity.
- In all irons examined, hardness decreases with rising oxygen activity. The drop is most pronounced in the lower oxygen activity range.
- The change of various properties during magnesium fade is well known for quite long. However, oxygen activity measurement permits to follow these changes quite accurately during production and not afterwards on the castings produced. Indeed, oxygen activity directly reflects instantaneous chemical equilibrium between oxygen, sulfur and magnesium (activity). Residual magnesium measured on solidified castings does not offer this opportunity.

This article is based on an paper presented at the WFO Technical Forum on June 12 to 14, 2007 in Düsseldorf, Germany

Literature

[1] Hofmann, E.; Wolf, G.: Reproduzierbare Herstellung von Gusseisen mit Vermiculargraphit unter Verwendung einer verbesserten EMK-Messtechnik. Giessereiforschung 53 (2001) no. 4, pp. 131-151.
[2] Lerner, Y.: Titanium in the rapidly cooled hypereutectic gray iron. Materials Engineering and Performance 12 (2003), pp. 141-146.
[3] Hecht, M.; Loury, J. B.: Determination and significance of oxygen activity in baths of cast iron treated with magnesium. Fonderie 204 (2001), pp. 12-32.
[4] Hummer, R.: Die Sauerstoffaktivität, ein Qualitätsmerkmal von Gusseisen – ein Überblick mit Hinweisen auf ein neues Anwendungsgebiet. Giesserei-Rundschau 50 (2003) no. 9/10, pp. 220-226.
[5] Hummer, R.: Schmelzekontrolle von Mg-behandelten Gusseisenschmelzen mit Hilfe von EMK-Messungen. 58th World Foundry Congress, Krakow, Poland, paper 2, 1991.
[6] Morinaka, M.; Okuzono, T.: Graphite shape control factors in cast iron. Chuzo-kogaku. Journal of Japan Foundry Engineering Society 73 (2001), no. 8, pp. 512-516.
[7] HEN foundry sensor: Heraeus Electro-Nite Celox-Foundry, CF 10100692.

[8] Fray, D. J.: The use of solid electrolytes in the determination of activities and the development of sensors. Metallurgical and Materials Transactions B 34B (2003), pp. 589-594.
[9] Mampaey, F.; Beghyn, K.: Oxygen activity in cast iron measured in induction furnace at variable temperature. AFS Transactions 114 (2006), paper no 06-115.
[10] Engh, T. A.: Principles of metal refining. Oxford Univ. Press, Oxford (1992).
[11] Mihajlovic, A.: Einfluss des gelösten Sauerstoffs auf das metallurgische Verhalten von kohlenstoffreichen Fe-C-O- bzw. Fe-C-Si-O-Schmelzen bei hohen und tiefen Temperaturen. Giesserei-Praxis (1976), no. 3, pp. 23-30.
[12] Wang, J.; Zhao, W.: Effects of oxygen on the solidification, microstructure and mechanical properties of cast irons. Japan Foundrymen's Soc. Proc. of the 2nd Asian Foundry Congress (1994). Pp. 25-29.
[13] Kim, E.-J.; You, B.-D.; Pak, J.-J.: Thermodynamics of carbon in liquid manganese and ferromanganese alloys. Metall. Materials Trans. 34B (2003), pp. 51-59.
[14] Mampaey, F.: A comparative study of nucleation in lamellar and spheroidal graphite cast iron, modeling of casting, welding and advanced solidification processes – V. Ed.: Rappaz, M.; Ozgu, M. R.; Mahin, K. W.: TMS Warrendale, 1991. Pp. 403-410.
[15] Chisamera, M.; Riposan, I.; Stan, S.; Skaland, T.: Undercooling – chill size – structure relationship in the Ca/Sr inoculated grey irons under sulphur/oxygen influence. World Foundry Congress Paris, 2000, paper RO 62.
[16] Skaland, T.; Grong, Ø.; Grong, T.: A Model for the graphite formation in ductile cast iron. Part I. Inoculation Mechanisms. Metallurgical Transactions 24A (1993), pp. 2321-2345.
[17] Orths, K.; Weis, W.; Lampic, M.: Verdeckte Fehler bei Gussstücken aus Gusseisen – Stand der Kenntnisse über die Ursachen und Versuche zur Klärung der Zusammenhänge. Giessereiforschung 27 (1975) no. 3, pp. 103-111.
[18] Merz, R.; Marinček, B.: Zur Oxydhautbildung verschiedener Roh- und Gusseisenschmelzen. Stahl und Eisen 75 (1955), no. 4, pp. 196-199.
[19] Orths, K.; Weis, W.; Lampic, M.: Einflüsse von Formstoff und Form, Schmelzführung und Desoxidation auf die Entstehung verdeckter Fehler bei Gusseisen. Giessereiforschung 27 (1975) no. 4, pp 113-128.
[20] Ghorpade, S.; Heine, R. W.; Loper, C. R. Jr.: Oxygen probe measurements in cast irons. AFS Transactions 83 (1975), pp. 193-198.
[21] Kusakawa, T.: Behavior of oxygen and nucleation of graphite in production of spheroidal graphite cast iron. Physical Metallurgy of Cast Iron V, Scitec Publications, Ueticon-Zuerich, 1997. Pp. 61-72.
[22] Höner, K. E.; Baliktay, S.: Einige Betrachtungen zur Reduktion von Silicium aus fester Kieselsäure durch in Eisenschmelzen gelösten Kohlenstoff. Giessereiforschung 25 (1973) no. 1, pp. 21-27.
[23] Hrusovski, J. P.; Wallace, J. F.: Effect of composition on solidification of compacted graphite iron. AFS Transactions 93 (1985), pp. 55-86.
[24] Müller, J.; Siefer, W.: Menge und Bindungsformen des Sauerstoffs in Einsatzmaterialien, Gusseisen und Stahlguss sowie Hinweise zur Identifizierung verdeckter Fehler. Giessereiforschung 42 (1990) no 4, pp. 183-202.
[25] Labreque, C.; Gagné, M.; Planque, E.: Effect of charge materials on slag formation in ductile iron melts. Keith Millis World Symposium on Ductile Iron, 2003, American Foundry Soc. Pp. 41-48.
[26] Kusakawa T.; Xu, X.; Okimoto, S.: Effects of oxygen in cast iron during melting and solidification process. Report of the castings research laboratory, Waseda University, no. 38, 1988. Pp. 33-39.
[27] McLean, A.: The science and technology of steelmaking – measurements, models, and manufacturing. Metallurgical & Materials Transactions 37B (2006), Pp. 319-332.
[28] Itofuji, H.: The influence of free magnesium on some properties in spheroidal graphite irons. Int. J. Cast Metals Res. 12 (1999), pp. 179-187.
[29] Mampaey, F.: Image analysis of graphite particles by a mathematical description of the particle contour: AFS Transactions 113, paper no 05-155 (2005) (B).
[30] Mampaey, F.: Acoustic resonance analysis for examining the graphite shape in cast iron. Accepted for publication in AFS Transactions 114 (2007), paper no. 07-129.
[31] Mampaey, F.: Aluminum cast irons: Solidification, feeding and oxygen activities. AFS Transactions 113 (2005), paper no. 05-149.
[32] Lekakh, S.; Loper, C. R. Jr.: Improving inoculation of ductile iron. AFS Transactions 2003 Paper 03-103, pp. 1-10.
[33] Skaland, T.: A new approach to ductile iron inoculation. AFS Transactions (2001), paper 01-078, pp: 1-12.

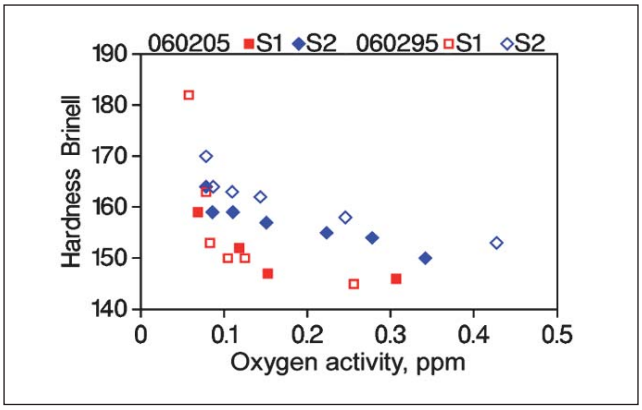

Figure 30: In ferritic irons, hardness decreases with rising oxygen activity.

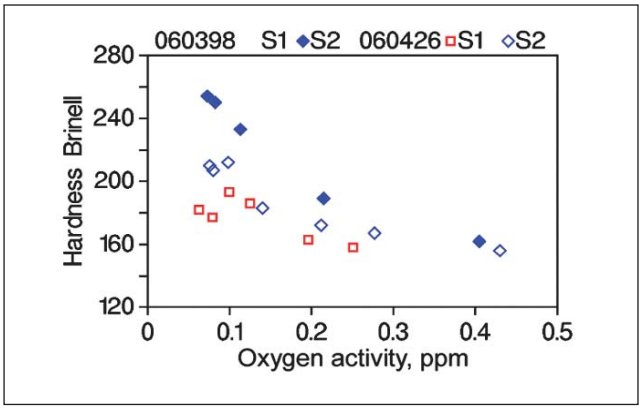

Figure 31: In irons with mixed ferritic-pearlitic matrix hardness decreases with rising oxygen activity.

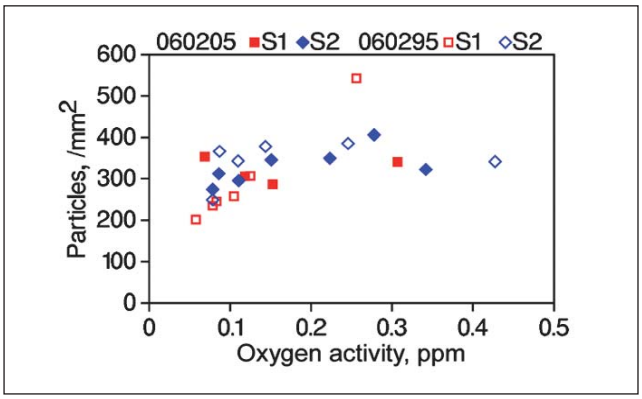

Figure 32: Graphite particle count versus oxygen activity obtained in ferritic irons

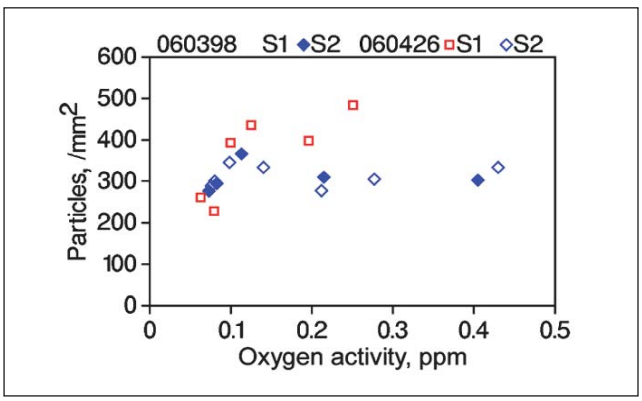

Figure 33: Graphite particle count versus oxygen activity obtained in irons with mixed ferritic-pearlitic matrix

Heraeus

Heraeus Electro-Nite GmbH & Co. KG
Im Stift 6-8
D-58119 Hagen
Tel. +49 2334 955-6
Fax. + 49 2334 955-800
info.electro-nite.de@heraeus.com
www.electro-nite.de

Heraeus Electro-Nite International N.V.
Centrum Zuid 1105
B-3530 Houthalen, Belgium
Tel. +32 11 600-211
Fax. + 32 11 600-400
info.electro-nite.be@heraeus.com
www.electro-nite.be

Heraeus Electro-Nite Co.
One Summit Square
1st Floor, Suite 100
Langhorne, PA 19047
TEL 1 215 944 9000
FAX 1 215 860 6657
info.electro-nite.us@heraeus.com

Electro-Nite